



## RESEARCH ARTICLE

10.1029/2019JD031339

## Special Section:

Carbon and Weather: Results from the Atmospheric Carbon and Transport – America Mission

## Key Points:

- Multispecies flask samples are used to characterize regional wintertime eastern U.S. CO<sub>2</sub> and CH<sub>4</sub> enhancement variability
- Mid-Atlantic and Midwestern U.S. CO<sub>2</sub> and CH<sub>4</sub> enhancements are primarily anthropogenic
- Winter Southeastern U.S. CO<sub>2</sub> and CH<sub>4</sub> enhancements indicate influence from biogenic exchange and surface processing

## Correspondence to:

B. C. Baier,  
bianca.baier@noaa.gov

## Citation:

Baier, B. C., Sweeney, C., Choi, Y., Davis, K. J., DiGangi, J. P., Feng, S., et al. (2020). Multispecies assessment of factors influencing regional CO<sub>2</sub> and CH<sub>4</sub> enhancements during the winter 2017 ACT-America campaign. *Journal of Geophysical Research: Atmospheres*, 125, e2019JD031339. <https://doi.org/10.1029/2019JD031339>

Received 11 JUL 2019

Accepted 25 DEC 2019

Accepted article online 27 DEC 2019

## Multispecies Assessment of Factors Influencing Regional CO<sub>2</sub> and CH<sub>4</sub> Enhancements During the Winter 2017 ACT-America Campaign

Bianca C. Baier<sup>1,2</sup>, Colm Sweeney<sup>2</sup>, Yonghoon Choi<sup>3</sup>, Kenneth J. Davis<sup>4,5</sup>, Joshua P. DiGangi<sup>3</sup>, Sha Feng<sup>4</sup>, Alan Fried<sup>6</sup>, Hannah Halliday<sup>3</sup>, Jack Higgs<sup>1</sup>, Thomas Lauvaux<sup>4</sup>, Benjamin R. Miller<sup>1,2</sup>, Stephen A. Montzka<sup>1</sup>, Timothy Newberger<sup>1,2</sup>, John B. Nowak<sup>1</sup>, Prabir Patra<sup>7</sup>, Dirk Richter<sup>6</sup>, James Walega<sup>6</sup>, and Petter Weibring<sup>6</sup>

<sup>1</sup>Cooperative Institute for Research in Environmental Sciences, University of Colorado-Boulder, Boulder, CO, USA, <sup>2</sup>NOAA Earth System Research Laboratory Global Monitoring Division, Boulder, CO, USA, <sup>3</sup>NASA Langley Research Center, Hampton, VA, USA, <sup>4</sup>Department of Meteorology and Atmospheric Science, Pennsylvania State University, University Park, PA, USA, <sup>5</sup>Earth and Environmental Systems Institute, Pennsylvania State University, University Park, PA, USA, <sup>6</sup>Institute for Alpine and Arctic Research, University of Colorado-Boulder, Boulder, CO, USA, <sup>7</sup>Japan Agency for Marine-Earth Science and Technology, Kaganawa, Japan

**Abstract** Diagnosing carbon dioxide (CO<sub>2</sub>) and methane (CH<sub>4</sub>) fluxes at subcontinental scales is complicated by sparse observations, limited knowledge of prior fluxes and their uncertainties, and background and transport errors. Multispecies measurements in flasks sampled during the wintertime ACT-America campaign were used for background characterization and source apportionment of regional anthropogenic CO<sub>2</sub> and CH<sub>4</sub> fluxes when ecosystem CO<sub>2</sub> exchange is likely to be least active. Continental background trace gas mole fractions for regional enhancements are defined using samples from the upper troposphere and assessed using model products. Trace gas enhancements taken from flask samples in the lower troposphere with background levels subtracted out are then interpreted to inform CO<sub>2</sub> and CH<sub>4</sub> enhancement variability in the eastern United States. Strong correlations between CO<sub>2</sub> and CH<sub>4</sub> enhancements in the Midwestern and Mid-Atlantic United States indicated colocated anthropogenic sources. Oil and natural gas influence was also broadly observed throughout the entire observational domain. In the Midwestern United States, agricultural influence on CO<sub>2</sub> and CH<sub>4</sub> enhancement variability was evident during above-average wintertime temperatures. Weaker correlations between CO<sub>2</sub> and anthropogenic tracer enhancements in the Southeastern United States indicated potentially nonnegligible wintertime ecosystem CO<sub>2</sub> exchange, with biogenic tracers indicating more active surface processing than other regions. These whole-air flask samples illuminated significant regional CO<sub>2</sub> and CH<sub>4</sub> sources or sinks during Atmospheric Carbon and Transport-America (ACT-America) and can provide additional information for informing regional inverse modeling efforts.

### 1. Introduction

Carbon dioxide (CO<sub>2</sub>) and methane (CH<sub>4</sub>) are the two most important atmospheric greenhouse gases because of their high growth rate and relative impact on the Earth's radiative balance (Ciais et al., 2014). Accurately quantifying CO<sub>2</sub> and CH<sub>4</sub> fluxes between terrestrial ecosystems and the atmosphere is therefore crucial for climate prediction. Atmospheric inversions of mole fraction measurements are used to infer CO<sub>2</sub> and CH<sub>4</sub> fluxes based on prior knowledge of sources or sinks (Bousquet et al., 1999; Tans et al., 1990). While inverse models have significantly contributed to knowledge of CO<sub>2</sub> and CH<sub>4</sub> fluxes over broad latitudinal bands (Bousquet et al., 2000; Francey et al., 1995; Tans et al., 1990), using inverse methods to constrain the carbon cycle on subcontinental scales is more difficult (Chevallier et al., 2010; Gurney et al., 2002; Huntzinger et al., 2012; King et al., 2015; Lauvaux et al., 2009, 2012a; Peylin et al., 2013; Rödenbeck et al., 2003). The accuracy achievable with inverse analyses is limited by sparse atmospheric observations available to constrain inverse models (Ciais et al., 2010; Gloor et al., 2000; Göckede et al., 2010; Gurney et al., 2002, 2003); poorly quantified and potentially large uncertainties in tracer transport (Baker et al., 2006; Chevallier et al., 2010; Díaz-Isaac et al., 2018; Gurney et al., 2003; Isaac et al., 2014; Lauvaux & Davis, 2014; Schuh et al., 2019; Stephens et al., 2007); limited knowledge of prior fluxes—especially from the terrestrial

biosphere (Hayes et al., 2011; Huntzinger et al., 2012; King et al., 2012); and uncertainties in background levels (Göckede et al., 2010; Gourdjji et al., 2012; Lauvaux et al., 2012b; Schuh et al., 2010). CO<sub>2</sub> and CH<sub>4</sub> emissions mitigation effectiveness will benefit from reduced uncertainties in these regional inverse flux estimates.

Comprehensive, regional-scale attribution of prior CO<sub>2</sub> and CH<sub>4</sub> fluxes from both natural and anthropogenic sources can reduce inverse flux uncertainties. Primary sources of anthropogenic CH<sub>4</sub> emissions are the energy (coal mining, oil, and natural gas operations), waste management, and agricultural industries. Its largest natural source is wetland emissions (Birdsey et al., 2018). Anthropogenic CO<sub>2</sub> is primarily emitted through fossil fuel combustion. While CH<sub>4</sub> has small atmospheric sinks to hydroxyl radical oxidation (Levy, 1971) and enzyme mediation in the subsoil (Born et al., 1990), net ecosystem-atmosphere exchange of CO<sub>2</sub> involves competing fluxes from both photosynthesis and respiration (Birdsey et al., 2018). Quantifying regional-scale CO<sub>2</sub> and CH<sub>4</sub> fluxes remains challenging for scientists, and the disagreement between top-down and bottom-up (process-level) emissions estimates can be large (Brandt et al., 2014; King et al., 2015). One approach to emissions attribution is to examine the relationship between CO<sub>2</sub>, CH<sub>4</sub>, and other source-specific, coemitted trace gases (tracers). Comeasured tracers such as nonmethane hydrocarbons, halocarbons, and stable carbon isotopes have proven valuable for assessing atmospheric composition and carbon emissions throughout the United States (Choi et al., 2008; Guha et al., 2015; Miller et al., 2012; Peischl et al., 2013; Pétron et al., 2012; Smith et al., 2017; Turnbull et al., 2014). Ethane and propane are tracers for CH<sub>4</sub> emissions from the oil and natural gas sector (Cambaliza et al., 2015; Miller et al., 2013; Peischl et al., 2013; Plant et al., 2019). The radiocarbon content of CO<sub>2</sub> (<sup>14</sup>CO<sub>2</sub>) is used extensively to derive recently added fossil fuel CO<sub>2</sub> (LaFranchi et al., 2013; Levin et al., 1989; Miller et al., 2012; Schwietzke et al., 2014; Turnbull et al., 2011, 2014). Carbonyl sulfide, methyl halides, or combustion byproducts are tracers for photosynthetic uptake (Blake et al., 2008; Montzka et al., 2007), wetland and biomass burning emissions (Andreae & Merlet, 2001), and urban emissions (Choi et al., 2008; Turnbull et al., 2019), respectively. Whole-air sampling provides a large suite of tracers that are measured on calibrated instruments in a laboratory-controlled environment, ensuring compatibility with other global mole fraction tracer measurements. Although less spatially and temporally resolved than continuous measurements, discrete samples can help to characterize regional CO<sub>2</sub> and CH<sub>4</sub> sources.

Small changes in CO<sub>2</sub> and CH<sub>4</sub> mole fractions from surface fluxes are superimposed onto large background mole fractions. Source attribution requires the decoupling of regional mole fraction enhancements (or depletions) from continental background conditions. Continental- to regional-scale studies have used remote, stable surface observations (i.e., those not influenced by local emissions) (Masarie & Tans, 1995; Thoning et al., 1989) and observations in the upper troposphere (UT) (Chang et al., 2014; Graven et al., 2009; Lan et al., 2019; Miller et al., 2012; Turnbull et al., 2006; Zhao et al., 2009) to derive background CO<sub>2</sub> and CH<sub>4</sub> levels. Others combined observations and model output at domain boundaries (Barkley et al., 2017; Gerbig et al., 2003; Gourdjji et al., 2012; Hu et al., 2015; Jeong et al., 2013; Kort et al., 2008; Lauvaux et al., 2012b; Miller et al., 2013; Zhao et al., 2009). In general, incorrectly disaggregating regional mole fractions from background levels can lead to biased flux estimates and improper attribution of CO<sub>2</sub> and CH<sub>4</sub> enhancements to surface sources or sinks (Cambaliza et al., 2014; Graven et al., 2009; Hu et al., 2015; Lauvaux et al., 2012a; Schuh et al., 2010; Turnbull et al., 2014).

The Atmospheric Carbon and Transport-America (ACT-America) mission provided a unique opportunity to interpret seasonal CO<sub>2</sub>, CH<sub>4</sub>, and other trace gas enhancements in three eastern U.S. regions. Five, 6-week airborne campaigns between summer 2016 and summer 2019 obtained high-density in situ and remotely-sensed CO<sub>2</sub> and CH<sub>4</sub> across various synoptic regimes and surface source regions. This work focuses on the interpretation of flask samples analyzed for a suite of trace gases for regional, anthropogenic CO<sub>2</sub>, and CH<sub>4</sub> source characterization during winter 2017 when CO<sub>2</sub> attribution is least likely to be influenced by active ecosystem exchange. Flask samples in the UT were used to define background conditions and to calculate multispecies enhancements. The implications of using the UT as a background were assessed using observations at remote sites within North America and simulated mole fractions from two global model products. Finally, CO<sub>2</sub> and CH<sub>4</sub> enhancements were qualitatively interpreted for source apportionment within the ACT-America domain by using comeasured trace gases in flask samples.

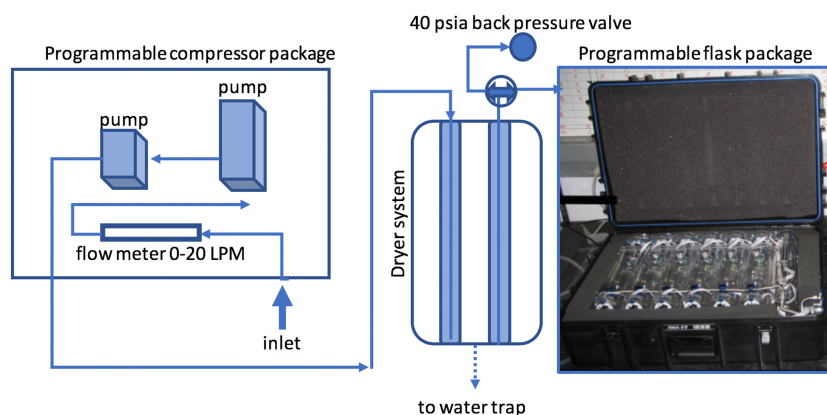


**Figure 1.** Ambient air is pulled through a stainless steel inlet via the programmable compressor package and dried using a gas chiller situated between the programmable compressor and flask packages. Arrows indicate the direction of airflow through the flask sampling system.

## 2. Data and Methods

### 2.1. Measurement Domain and Platforms

The NASA C-130 and B-200 airborne platforms acquired trace gas mole fraction measurements in the eastern United States during ACT-America. Flights were conducted out of the Mid-Atlantic (Wallops Island, VA), the Midwest (Lincoln, NE), and the Southeastern United States (Shreveport, LA). Each region encompasses various biomes and large anthropogenic CO<sub>2</sub> and CH<sub>4</sub> sources: The Mid-Atlantic region includes heavily forested areas, oil and gas extraction zones, and urban centers with dense fossil fuel emissions; the Midwest region is the agricultural center of the United States and is bordered by shale plays; and the Southeastern region is surrounded by oil and gas extraction zones, urban hotspots, agricultural regions, and coastal wetlands. Both remote and in situ aircraft sensors measured CO<sub>2</sub> and CH<sub>4</sub> alongside other select atmospheric trace gases and meteorological variables. Flask sampling and continuous in situ observation methods are described here; other available measurements are archived online (at <https://daac.ornl.gov>).

### 2.2. Flask Systems and Sampling Strategy

NOAA/Earth System Research Laboratory (ESRL) Global Monitoring Division flask packages were installed on each aircraft during ACT-America. Routinely used in the Carbon Cycle and Greenhouse Gases (CCGG) aircraft network (Sweeney et al., 2015), these portable systems include a programmable flask package (PFP), a programmable compressor package, and a data logging and control package (Figure 1). Packages consist of twelve 0.7-L borosilicate glass flasks that are pressurized to 275 kPa (40 psia) for a total sample volume of ~2.2 L. Each flask is filled by pulling ambient air through a stainless steel inlet using two pumps within the compressor package. These pumps are plumbed in series to ensure both high flow rates and sufficient flask pressurization to 275 kPa at low pressure altitudes. During winter 2017, a gas chiller was installed between the compressor package and PFPs that dried air samples to less than 1% absolute humidity. Details on sample drying are discussed in section 2.3.1. Sampling system components downstream of the dryer were flushed with dried ambient air prior to flask fill, and diagnostic data were logged every 10 s during the filling. A thorough description of the flask sampling setup and procedures is described in Sweeney et al. (2015).

Flask samples were returned to NOAA/ESRL's Global Monitoring Division in Boulder, CO, for analysis. A first sample air aliquot was analyzed on a custom-built system (Measurement of Atmospheric Gases that Influence Climate Change, MAGICC) for dry air mole fraction measurements of greenhouse gases including CO<sub>2</sub> and CH<sub>4</sub>, and other long-lived atmospheric species (<https://www.esrl.noaa.gov/gmd/ccgg/aircraft/analysis.html>). MAGICC gases were calibrated to standard scales maintained at NOAA/ESRL (Dlugokencky et al., 2005; Hall et al., 2007; Novelli et al., 1991; Zhao & Tans, 2006). A second aliquot was analyzed on the PERSEUS GC/MS (PR1) system for over 50 other nonmethane hydrocarbons, halocarbons, and other sulfur-containing compounds. All PR1 analyses are reported on NOAA absolute calibration scales, derived in-house from pure components and high-precision gravimetric techniques. The remaining flask sample air was transferred to the Institute of Arctic and Alpine Research (INSTAAR) at the University of Colorado-Boulder for stable carbon isotope measurements and, for selected samples, CO<sub>2</sub> graphitization

**Table 1**  
*Flask Species Used for Source Attribution*

Chemical formula, species name	Lower troposphere (<1,500 m MSL) Median (ppt)	1 $\sigma$ Unc. <sup>a</sup>
<i>MAGICC analysis system:</i>		
CO, carbon monoxide	148.9 ppb	0.8 ppb
CO <sub>2</sub> , carbon dioxide	413.5 ppm	0.06 ppm
CH <sub>4</sub> , methane	1,960.7 ppb	1.06 ppb
N <sub>2</sub> O, nitrous oxide	330.3 ppb	0.3 ppb
SF <sub>6</sub> , sulfur hexafluoride	9.37	0.04
H <sub>2</sub> , molecular hydrogen	499.3 ppb	1.8 ppb
<i>HATS PR1 Analysis System:</i>		
C <sub>2</sub> H <sub>2</sub> , acetylene	458.1	2.1
C <sub>2</sub> H <sub>6</sub> , ethane	2,920.6	12
C <sub>3</sub> H <sub>8</sub> , propane	1,201.6	5.5
i-C <sub>4</sub> H <sub>10</sub> , i-butane	181.0	1.9
n-C <sub>4</sub> H <sub>10</sub> , n-butane	339.2	1.7
i-C <sub>5</sub> H <sub>12</sub> , i-pentane	100.3	1.8
n-C <sub>5</sub> H <sub>12</sub> , n-pentane	82.1	1.2
C <sub>6</sub> H <sub>6</sub> , benzene	116.9	1.4
CH <sub>3</sub> Br, methyl bromide	6.81	0.06
CH <sub>3</sub> Cl, methyl chloride	561.3	1.3
OCS, carbonyl sulfide	514.5	4.3

*Note.* MAGICC = Measurement of Atmospheric Gases that Influence Climate Change; HATS = Halocarbons and other Atmospheric Trace Species group within NOAA/ESRL. Median lower-tropospheric mole fractions are reported for the 2017 ACT-America wintertime deployment. Uncertainties in HATS PR1 analysis system gases are the 1 $\sigma$  standard deviation of flask species measurements after undergoing long-term (>30 days) storage but also implicitly include influences from HATS instrument nonlinearity corrections, system blank contamination, and both detector and standard drifting. Uncertainties in MAGICC species are expressed as the 1 $\sigma$  standard deviation in measurements after undergoing long-term (>28 days) storage testing (Sweeney et al., 2015). Variability induced by storage is the largest source of uncertainty, but as analysis occurred within 2 weeks of sampling, uncertainties are conservative.

<sup>a</sup>Uncertainties reported in parts per trillion (ppt) unless otherwise labeled.

in preparation for radiocarbon (<sup>14</sup>CO<sub>2</sub>) measurements. Analytes used here are listed in Table 1 with their associated uncertainties.

Twenty-five total research flights conducted between February and March 2017 surveyed trace gases from the surface to approximately 8 km. In-flight hours spanned 11:00 to 18:00 local time to sample a well-developed atmospheric boundary layer. Flights were conducted under fair-weather conditions to quantify CO<sub>2</sub> and CH<sub>4</sub> emissions; transited frontal boundaries to assess mixing and transport of CO<sub>2</sub> and CH<sub>4</sub> mole fractions; and underflew the spaceborne Orbiting Carbon Observatory (OCO-2) to evaluate retrieved total column CO<sub>2</sub>. On average, 6 to 12 flasks were sampled on each flight (see Figure 2). A total of 332 flasks were analyzed, with 140 flasks sampled on fair-weather days and used for the analysis below. Flasks were sampled on level-altitude flight legs in various atmospheric layers: Most flasks were filled within the lower troposphere (LT), which contains the largest variability in CO<sub>2</sub> and CH<sub>4</sub> due to proximity to surface fluxes. The UT (~3,500–8,000 m MSL) was occasionally sampled to capture continental background air behavior, resulting in a LT:UT flask sample ratio of approximately 5:1 (Figure 2).

### 2.3. Flask Comparisons With Continuous Systems

Continuous four-species analyzers measured dry mole fractions of CO<sub>2</sub>, CH<sub>4</sub>, water vapor (H<sub>2</sub>O), and carbon monoxide (CO) at approximately 0.4 Hz via cavity ring-down spectroscopy on both aircraft. In-flight drift corrections were performed hourly while ground calibrations occurred weekly. All calibrations used NOAA/ESRL secondary standards that were tied to the World Meteorological Organization (WMO, WMO,

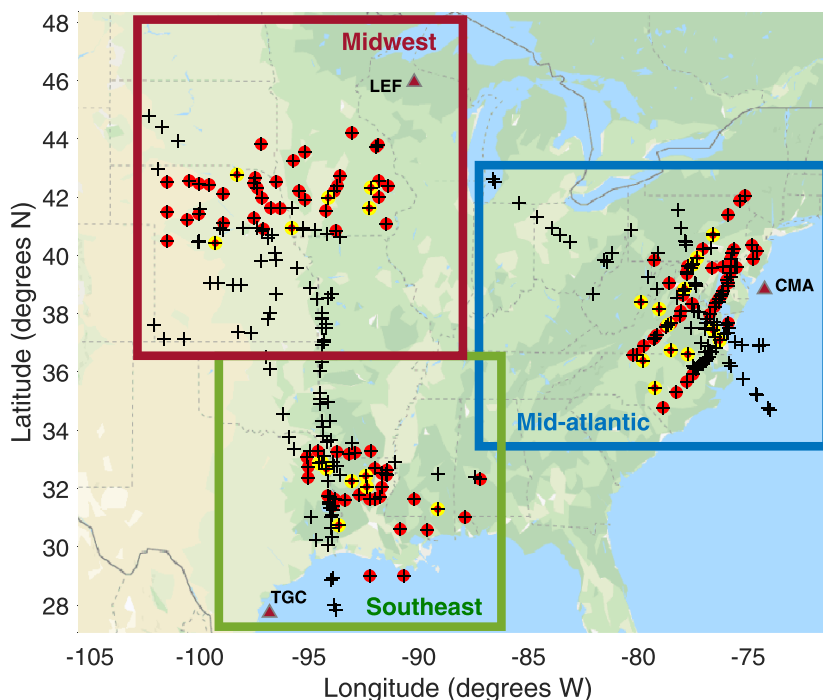


**Figure 2.** Winter 2017 flask sample locations within the ACT-America domain. Black pluses indicate all flask sample locations, with red points indicating fair-weather flask samples and yellow points indicating UT (>3,500 m MSL) samples. Maroon triangles indicate long-term NOAA CCGG aircraft flask sampling sites: Park Falls, WI (LEF), Cape May, NJ (CMA), and Corpus Christi, TX (TGC).

2013) scale. Details on these measurements can be found online (at <https://doi.org/10.3334/ORNLDAAAC/1556>).

The Compact Airborne Multi-Species Spectrometer (CAMS2) onboard the B-200 aircraft measured ethane ( $C_2H_6$ ) in situ by midinfrared absorption spectroscopy. Calibrations were performed before each flight using various ethane standards; in-flight, the instrument and inlet were zeroed every 5–7 min. Comprehensive details of this instrument, including calibration, zeroing, data acquisition and processing, and further in-flight comparisons with the PFP ethane samples, will be reported in a separate manuscript.

As flask samples were collected through a separate inlet but calibrated to the same WMO scale as the aforementioned sensors, flask-in situ comparisons provide a direct measure of the compatibility of these systems during ACT-America. Continuous and flask system comparisons were made by averaging the continuous measurements over a flask averaging “kernel.” Rather than interpolating the continuous measurements to flask fill end-times, a kernel was derived by optimizing an averaging window for continuous data between the flask start and end fill times to yield the strongest correlation between both flask and continuous trace gas ( $CO$ ,  $CH_4$ , and  $CO_2$ ) mole fractions. Correlations yielded  $R^2$  values greater than 0.98 when averaging the 1-Hz continuous data in a 15-s window prior to the flask fill end-time. Averaging times shorter than or beyond this window degrade correlations for all trace gases.

### 2.3.1. Water Vapor Artifacts

Comparisons between flask and continuous data presented for the summer 2016 ACT-America campaign underscore the need for sample drying. Comparisons (Figure 3a) indicated that flask samples exhibited  $CO_2$  depletion above  $\sim 1.7\%$  absolute humidity; other species exhibited no water vapor dependence. This artifact was recently discovered in NOAA/ESRL CCGG network flask-in situ comparisons for sites where air sample drying was not employed. Increased scatter in flask-in situ differences during periods of both high atmospheric variability and high humidity complicate the quantification of  $CO_2$  depletion in flasks. Excluding periods of high variability (i.e.,  $1\sigma$  in situ  $CO_2$  over the flask averaging window  $> 0.8$  ppm) results in  $CO_2$  depletion of 0.1 and 0.8 ppm at 1.75% and 3–4% absolute humidity, respectively. While a mechanism and empirical correction for this bias has not yet been identified, drying flask samples negated this artifact (Figure 3b).

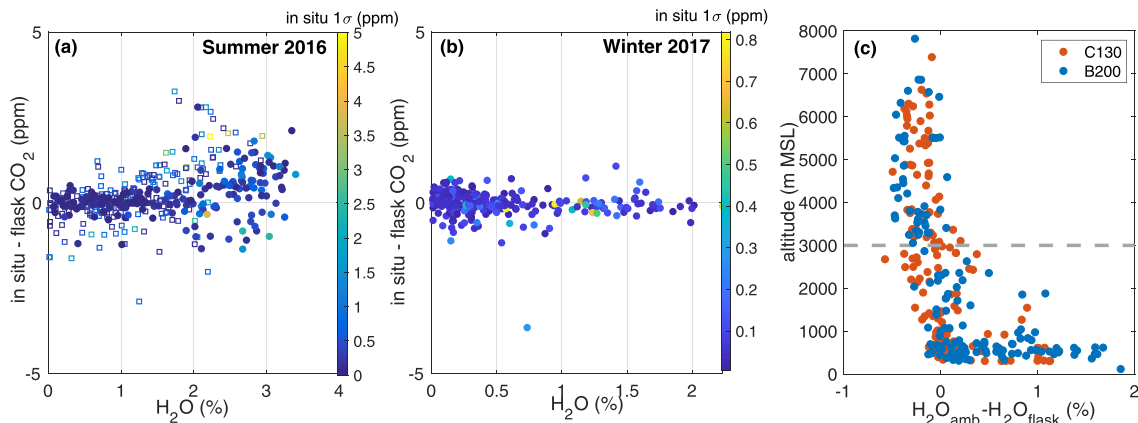


**Figure 3.** Differenced continuous and flask CO<sub>2</sub> as a function of absolute humidity. In panel (a), filled circles represent ACT-America summer 2016 differences, while open squares show NOAA/ESRL tower network in situ-flask differences during the same time period. Winter CO<sub>2</sub> differences after the chiller was added to the flask system are shown in (b). In panels (a) and (b), points are colored by the standard deviation in continuous measurements over the flask averaging kernel. Panel (c) shows the difference between flask and ambient absolute humidity levels versus altitude.

Flask samples were dried using a two-stage Peltier gas chiller (Figure 1) that decreased sample air temperatures to 5° C, condensing ambient water vapor into a vessel that was emptied after each flight. At altitudes below 3,000 m MSL, sample drying was enhanced by pressurizing the flask system upstream of and including the chiller to 40 psia. With sufficiently low atmospheric water vapor above this altitude threshold, pressurized drying was unnecessary. Water vapor content measured at the chiller output was below 1%, effectively negating CO<sub>2</sub> depletion (Figure 3b).

### 2.3.2. Wintertime Mole Fraction Comparisons

Comparisons of flask and continuous trace gas species are shown in Figure 4 as a function of mole fraction for all winter 2017 flights. Excluding periods of high atmospheric variability (e.g., continuous 1σ > 4 ppb CH<sub>4</sub>, >0.4 ppm CO<sub>2</sub>, >0.2 ppb C<sub>2</sub>H<sub>6</sub>, and >10 ppb CO over flask averaging window), offsets were generally within WMO comparability goals (2 ppb CH<sub>4</sub>, 0.05 ppm CO<sub>2</sub>, 1 ppb CO; WMO, 2013) and were within 0.1 ppb for C<sub>2</sub>H<sub>6</sub>. Mean offsets were similar for both aircraft platforms (Figure 4). However, standard deviations in these offsets can be large, and, similar to previous flask comparisons to continuous analyzers (Karion et al., 2013), when the data were more conservatively filtered (1σ > 2 ppb CH<sub>4</sub>, >0.2 ppm CO<sub>2</sub>, and >5 ppb CO), these offsets remained statistically significant. Higher-frequency logging of flask sampling was implemented

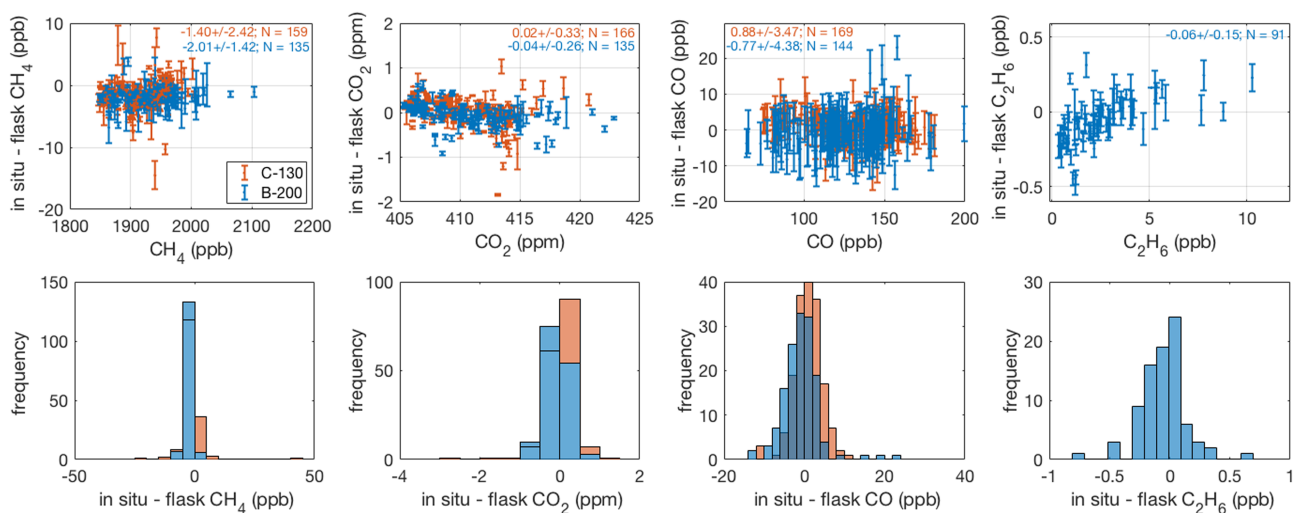


**Figure 4.** CH<sub>4</sub>, CO<sub>2</sub>, CO, and ethane (C<sub>2</sub>H<sub>6</sub>) continuous in situ minus flask mole fraction differences for each aircraft during winter 2017 versus in situ mole fraction. Error bars are standard deviations on the continuous measurements over the flask averaging kernel. Points are filtered to exclude high atmospheric variability and colored by aircraft, and mean offsets and standard deviations of differences are similarly colored.

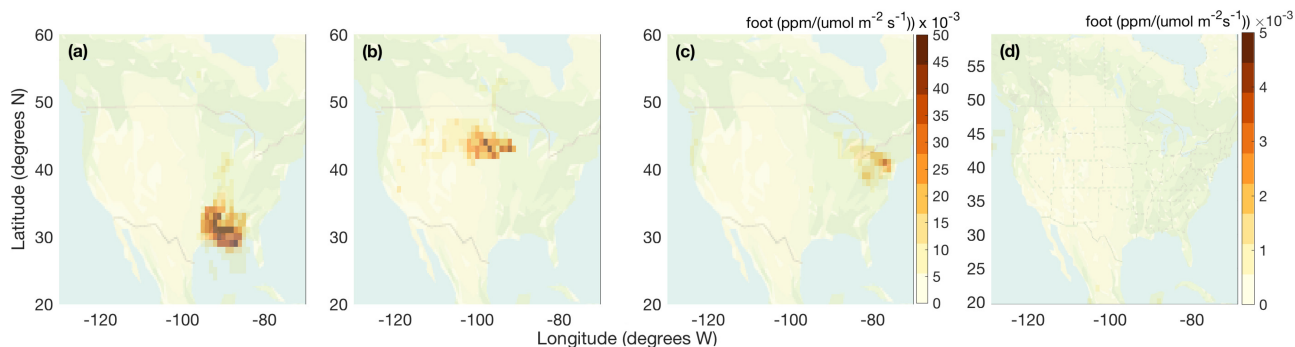


**Figure 5.** Total footprint in  $\text{ppm}/(\mu\text{mol}\cdot\text{m}^{-2}\cdot\text{s}^{-1})$  during winter 2017 for each ACT-America region (Southeast (a), Midwest (b), and Mid-Atlantic (c)) for fair-weather, lower-tropospheric ( $<1,500$  m MSL) flask receptors. The mean footprint for fair-weather, upper-tropospheric ( $>3,500$  m MSL) flask receptors for all three regions is shown in (d). Footprints were calculated from flask receptor locations on fair-weather days from HYSPLIT-WRF 500-particle, 10-day back trajectories.

in subsequent ACT-America campaigns to increase the accuracy and resolution of derived flask averaging kernels and to improve future comparisons.

A positive altitude dependence in the  $\text{CO}_2$  mole fraction comparisons was apparent in Figure 4 where offsets indicated a slight negative slope with increasing  $\text{CO}_2$  mole fraction. Typically, increased  $\text{CO}_2$  mole fractions at high altitude result from the combination of small leaks and slower flow rates at those altitudes. However, no leaks in the continuous  $\text{CO}_2$  systems were found at altitude. The entire flask system was leak checked multiple times throughout the campaign and did not indicate contamination. Flask systems were also tested before and after each campaign to ensure that the chiller and compressor did not impact trace gas mole fractions. Thus, the cause for the negative slope in the continuous and flask  $\text{CO}_2$  mole fraction offsets seen in Figure 4 remains unclear.

For ethane, comparisons between continuous and flask measurements yielded a positive slope of  $\sim 4\text{--}5\%$  (Figure 4). Further GC/MS and CAMS2 laboratory measurements of calibration standards performed after the ACT-America winter 2017 deployment indicated that the CAMS2 continuous ethane values are on average  $\sim 4.5\%$  higher than flasks. This offset is consistent with the positive slope in Figure 4.

#### 2.4. Footprint Calculation for Spatial Surface Influence

The Hybrid Single-Particle Lagrangian Integrated Trajectory (HYSPLIT) concentration dispersion model (Draxler & Hess, 1997) was used in Stochastic Time-Inverted Lagrangian Transport (STILT)-emulation mode to calculate surface influence functions (footprints) for each fair-weather flask sample location (hereby referred to as a “receptor”). HYSPLIT was driven with meteorological input from the Weather Research and Forecast (WRF) model (denoted HYSPLIT-WRF) and run backward for 10 days or until particles exit the North American continental boundary ( $\sim[-170, -90^\circ \text{W}]$  and  $\sim[20, 75^\circ \text{N}]$ ). For each trajectory, 500 particles were released at each flask receptor and tagged with a domain exit time and location (hereby referred to as an “endpoint”) to determine air mass origin. Footprints were generated every 15 min along the particle trajectory, aggregated, and separated into the three ACT-America study regions (Figure 5). Footprints calculated using HYSPLIT-WRF quantify the influence of both mixing processes and upwind emissions and are used to assess the region constrained by the flask trace gas species enhancements described in section 3.3.

#### 2.5. Background Estimation

Winter 2017 continental background mole fractions were defined from UT ( $>3,500$  m MSL) trace gas measurements in flasks (Figure 2). However, limited aircraft vertical profiling sometimes resulted in spatial and temporal inconsistency between UT and LT samples. Therefore, a single background mole fraction was calculated for each species in Table 1 by averaging all flask measurements in the UT ( $>3,500$  m MSL) for each day. Daily averaging of UT samples thereby simplifies defining background mole fractions on fair-weather flights, which avoided frontal boundaries and trace gas gradients within the UT. Flask and continuous observations yielded statistically similar daily standard deviations in UT  $\text{CO}_2$ ,  $\text{CH}_4$ , and CO mole fractions, indicating that UT variability is sufficiently represented by flask samples. We assume that the chemical composition of UT air is similar to that of the LT several days beforehand prior to the influence of regional surface sources or sinks. Any differences in temperature-dependent oxidation rates between the UT and LT

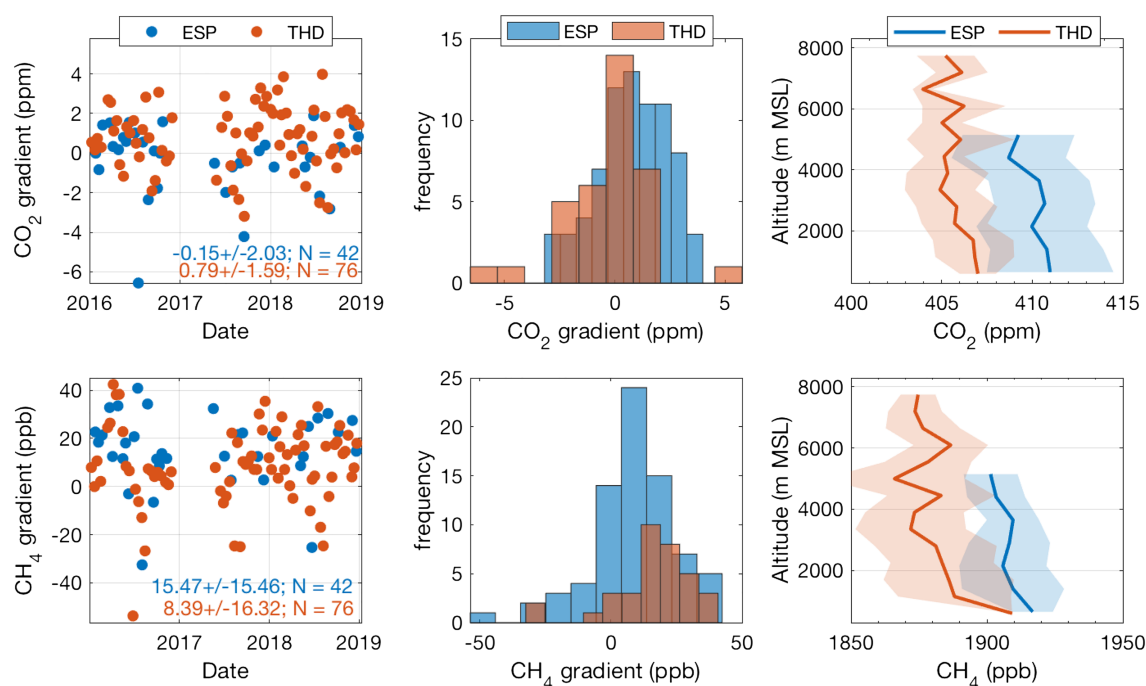


**Figure 6.** CO<sub>2</sub> and CH<sub>4</sub> vertical gradients [LT(<1,500 m MSL) minus UT (>3,500 m MSL)] observed at NOAA CCGG aircraft network sites, Trinidad Head, CA (THD) and Estevan Point (ESP), British Columbia (left) from 2016 to 2018. Measurements during winter 2017 were not available. Histograms of CO<sub>2</sub> and CH<sub>4</sub> vertical gradients for 2016–2018 at both sites are shown in middle panels. Observed CO<sub>2</sub> and CH<sub>4</sub> gradients for January–March 2016 and 2018 are shown on the right to indicate winter climatological CO<sub>2</sub> and CH<sub>4</sub> gradients typically observed upwind of the continent.

for trace gases considered here are assumed to be negligible over the transit time from the North American continental boundary (~days) relative to the wintertime lifetimes of these trace gases.

In section 3.2, we assess how well this UT background represents continental background levels for the LT using model distributions of CO<sub>2</sub> and CH<sub>4</sub>. CO<sub>2</sub> mole fractions were simulated by NOAA’s Carbon-Tracker, Version CT-NRT.v2018-1 (henceforth CT-NRT, Peters et al., 2007, with updates documented at <http://carbontracker.noaa.gov>). CT-NRT assimilates available CO<sub>2</sub> mole fraction observations worldwide to simulate global CO<sub>2</sub> fields. Global CH<sub>4</sub> mole fractions were simulated by the Atmospheric general circulation model driven Chemical Transport Model (ACTM; Patra et al., 2009). This forward model was driven with “online,” coupled chemistry and meteorology, and CH<sub>4</sub> emissions were derived from a climatological mean adjusted for the year 2017.

### 2.6. Wintertime Fair-Weather Enhancement Calculations

The subsequent analysis focuses on the interpretation of CO<sub>2</sub> and CH<sub>4</sub> enhancements during ACT-America winter 2017 fair-weather flights. Frontal weather flights were excluded due to large horizontal gradients in CO<sub>2</sub> and CH<sub>4</sub> observed throughout the atmospheric column at frontal boundaries, complicating the selection of UT air that is an appropriate background for the LT. Under fair weather, vertical mixing and convection are decreased; thus, UT air is hypothesized to be less influenced by surface fluxes.

Mole fraction measurements in flasks sampled below 1,500 m MSL were used to characterize the LT. Generally, the lowest altitude flight legs during ACT-America were planned to be within the atmospheric boundary layer. Regional trace gas enhancements above continental background levels (denoted by a Δ) for species in Table 1 were calculated by subtracting daily UT background mole fractions from LT ones. Flasks sampled between ~1,500 and ~3,500 m MSL were not used for enhancement calculations due to entrainment from the LT.

Enhancements likely exhibit some residual signal from vertical gradients at the continental boundary as observed at NOAA CCGG aircraft flask measurement sites, Estevan Point, British Columbia (49.3825° N, -126.5441° W) and Trinidad Head, CA (41.0541° N, -124.1510° W). To isolate regional trace gas enhancement signals from continental ones, enhancements are corrected to remove this “residual” gradient as in Lan et al. (2019) since over 80% of flask receptor air masses originated off of the western U.S. boundary near

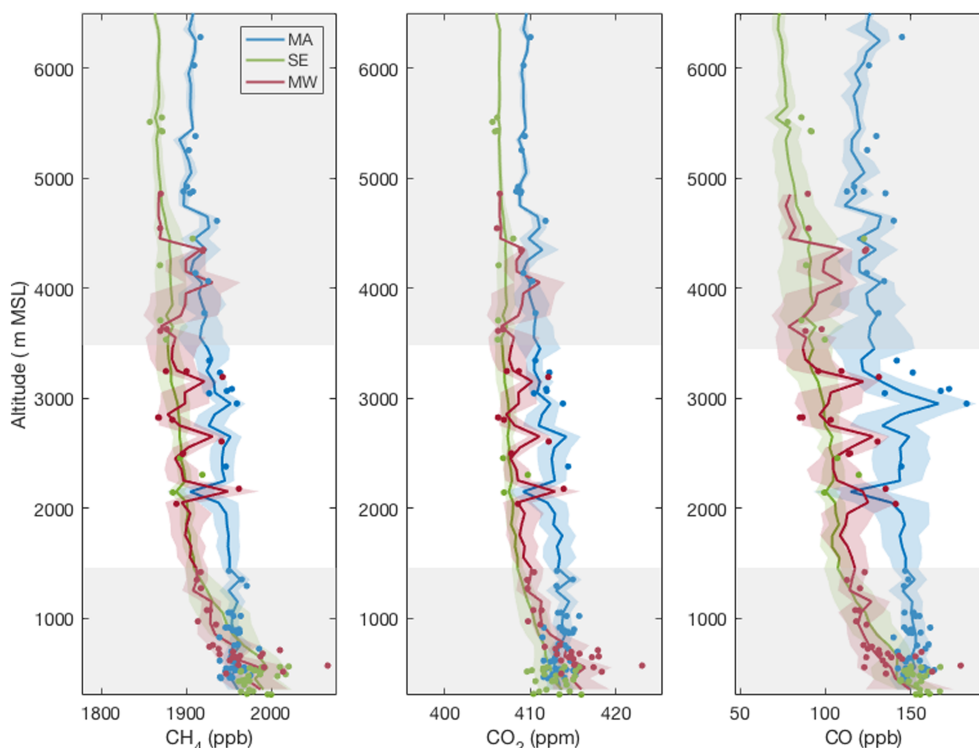


**Figure 7.** Continuous and flask fair-weather vertical distributions of  $\text{CH}_4$ ,  $\text{CO}_2$ , and  $\text{CO}$  for winter 2017. Continuous data are plotted as 100 m MSL binned medians (colored lines) with  $\pm 1\sigma$  standard deviation (colored shading). Flask sample mole fractions are plotted as discrete points at each sampling altitude and are similarly colored by region. Gray shading indicates altitude cutoffs for LT and UT flask samples as described in section 2.6.

these sites. A correction is calculated by averaging available wintertime measurements for clean, onshore flow conditions between January and March during 2016 and 2018 (Figure 6) and yields LT enhancements of  $+0.90 \pm 1.2$  ppm  $\text{CO}_2$  and  $+17.7 \pm 7.8$  ppb  $\text{CH}_4$ . Because ambient absolute humidity at these sites for winter 2016 and 2018 was below 1%, the residual  $\text{CO}_2$  gradient correction at Trinidad Head and Estevan Point was unaffected by flask  $\text{CO}_2$  water vapor artifacts discussed above.

### 3. Results and Discussion

#### 3.1. Greenhouse Gas Vertical Distributions

Vertical distributions of trace gases were examined throughout the partial atmospheric column on fair-weather days (Figure 7) with flasks sampled between 300 m MSL and 7,000 m MSL. The largest  $\text{CO}_2$ ,  $\text{CH}_4$ , and  $\text{CO}$  mole fractions were observed below 1,000 m MSL, indicating local surface sources, while decreased trace gas mole fractions in the UT are evidence of air that is less influenced by surface emissions. Although LT  $\text{CO}_2$  and  $\text{CH}_4$  levels were similar among regions, differences in UT  $\text{CO}_2$  and  $\text{CH}_4$  were apparent moving northeastward in the ACT-America domain. Wintertime UT mole fractions of  $\text{CO}_2$ ,  $\text{CH}_4$ , and  $\text{CO}$  in the northern United States increase over days to weeks due to the vertical propagation of seasonal changes in surface mole fractions. Similar wintertime integrated  $\text{CO}_2$ ,  $\text{CH}_4$ , and  $\text{CO}$  mole fraction enhancements in the northern United States relative to lower-latitude sites have been observed through sampling of the broader NOAA/ESRL aircraft network (Sweeney et al., 2015).

#### 3.2. Determining Long-Lived Trace Gas Enhancements

##### 3.2.1. Assessment of Upper-Tropospheric Background

Trace gas mole fractions sampled within the UT are used to define continental background air for the LT. We assess this background estimate using HYSPLIT-WRF particle back trajectories and simulated  $\text{CO}_2$  and  $\text{CH}_4$  fields from global model products (section 2.4). Simulated  $\text{CO}_2$  and  $\text{CH}_4$  mole fractions at back trajectory endpoints (i.e., locations upwind of the continent) from the CT-NRT  $\text{CO}_2$  inversion model and the ACTM  $\text{CH}_4$  forward model (section 2.5) are used to infer continental background  $\text{CO}_2$  and  $\text{CH}_4$  mole fractions prior to influence from regional emissions. Because CT-NRT  $\text{CO}_2$  is gridded at  $1^\circ \times 1^\circ$  resolution over CONUS,

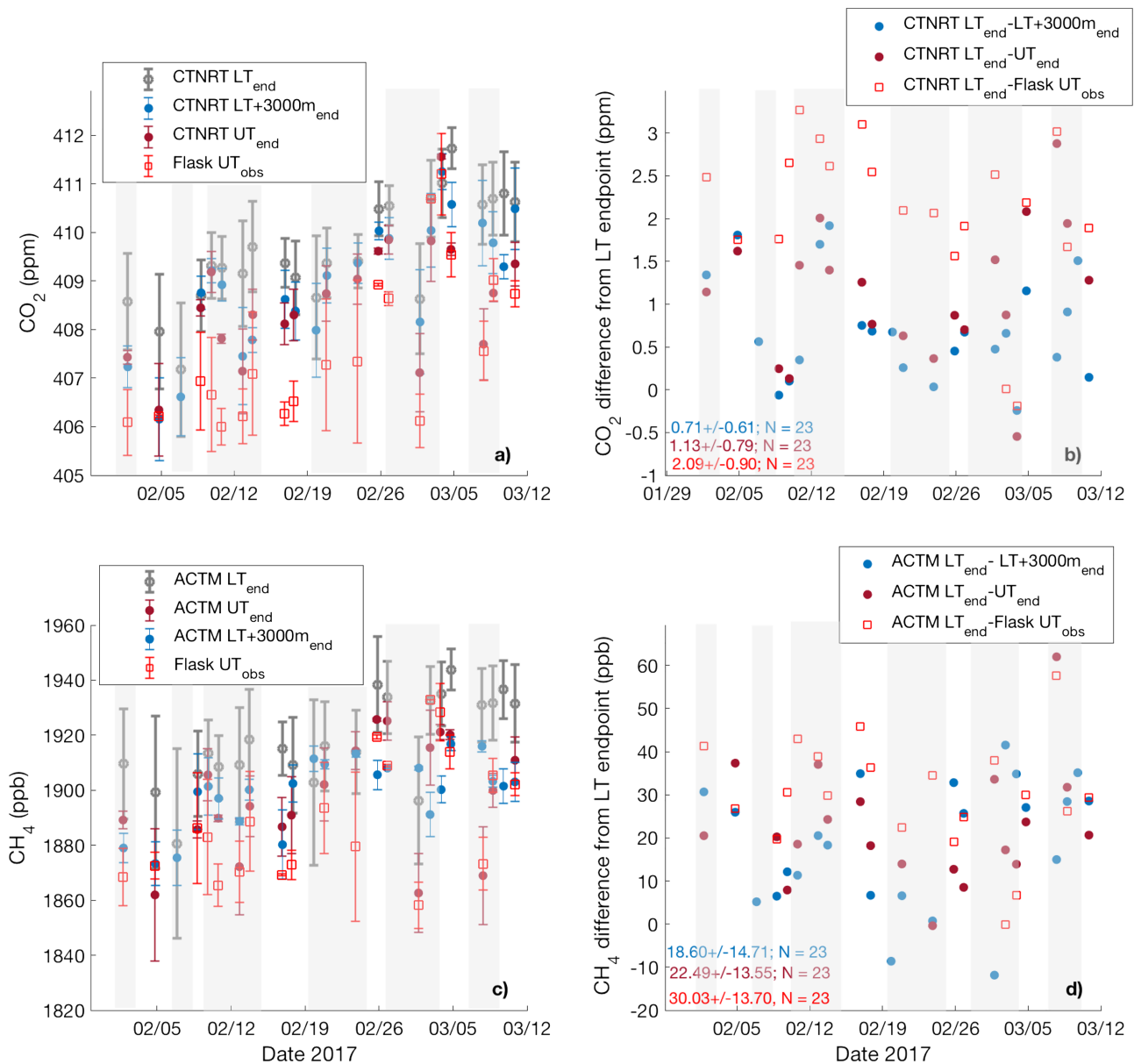


**Figure 8.** Simulated and observed endpoint mole fractions for all flight days. Shaded areas indicate frontal weather flights. Flask upper-tropospheric (UT<sub>obs</sub>) mole fractions for CO<sub>2</sub> (a) and CH<sub>4</sub> (c) are compared to those modeled at lower- (LT<sub>end</sub>) and upper-tropospheric (UT<sub>end</sub>) flask back trajectory endpoints by the CT-NRT inversion system and the ACTM, respectively. Error bars on simulated mole fractions indicate the mean 1 $\sigma$  standard deviation of CO<sub>2</sub> and CH<sub>4</sub> back trajectory endpoints across all 500 particles dispersed. Error bars on flask observations indicate the 1 $\sigma$  standard deviation in daily upper-tropospheric mole fractions. UT and LT mole fraction differences in (a) and (c) are shown in (b) and (d).

and both model products are gridded at roughly 3° × 2° globally, flask mole fractions will exhibit higher variability when compared to these lower resolution model products. The following criteria are examined to determine the representativeness of the average daily UT as a continental background: (1) There is no vertical gradient in the UT of the continental boundary, (2) vertical mixing of emissions from the surface into the UT does not contaminate background air, (3) the air mass origin for UT and LT flask samples during ACT-America are similar, and (4) there is no spatial gradient in the UT.

Trace gas vertical gradients observed within the UT during ACT-America (Figure 7) and at CCGG continental aircraft sites (Figure 6, third column) are weak relative to gradients observed between the UT and LT. This lack of vertical gradient above 3,500 m MSL suggests that daily mean background mole fractions derived from UT samples will not result in biased background estimates. Vertical mixing of surface flux-induced

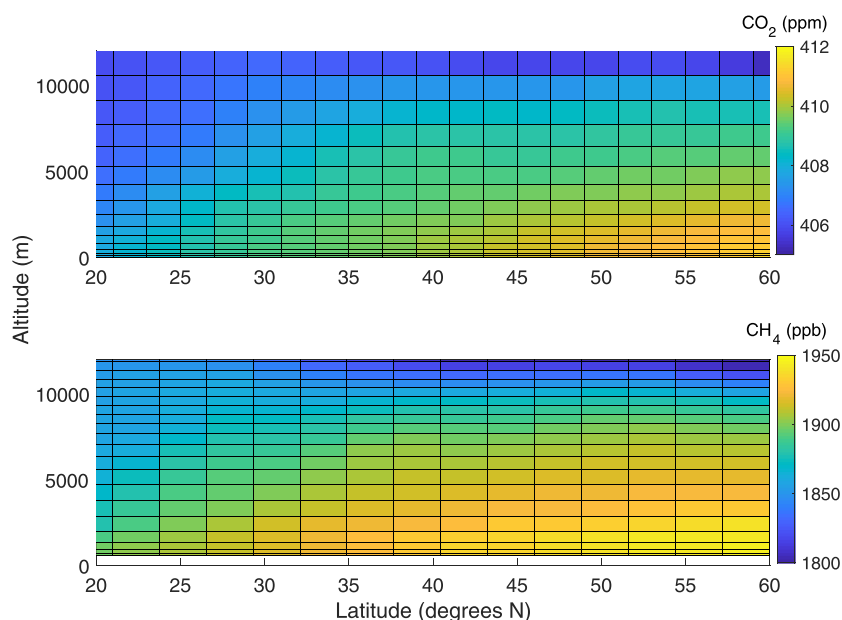


**Figure 9.** Average February 2017 CO<sub>2</sub> (top) and CH<sub>4</sub> (bottom) fields at 140° W longitude as a function of altitude and latitude. CO<sub>2</sub> and CH<sub>4</sub> fields were constructed from the CT-NRT and ACTM model products.

changes in mole fractions into the UT can also bias background estimates. However, analysis of the footprints calculated using HYSPLIT-WRF for LT and UT flask samples suggests an order of magnitude less surface influence above 3,500 m MSL during the wintertime (Figure 5). Therefore, UT contamination from surface fluxes during the wintertime is considered to be negligible.

Air mass origin for the UT can significantly affect estimated background CO<sub>2</sub> and CH<sub>4</sub> mole fractions due to large vertical and latitudinal gradients in CO<sub>2</sub> and CH<sub>4</sub> (Dlugokencky et al., 1994; Tans et al., 1990) and the seasonal positioning of these gradients. Further, if the upper and lower atmosphere are significantly decoupled, the UT may not be a well-suited background for the LT. Upwind mole fractions for flask receptor back trajectories intersecting 140° W are examined to determine if significant air mass origin differences exist between the UT and LT. We find model LT-UT differences of  $+1.13 \pm 0.79$  for CO<sub>2</sub> and  $+22.49 \pm 13.55$  ppb for CH<sub>4</sub> (Figure 8). When comparing simulated LT endpoint mole fractions to observed flask UT mole fractions for all flight days and assuming no vertical entrainment of surface fluxes, differences were  $+2.09 \pm 0.90$  ppm CO<sub>2</sub> and  $+30.03 \pm 13.70$  ppb CH<sub>4</sub>, which may reflect small inconsistencies in CT-NRT, ACTM and HYSPLIT-WRF transport, and/or errors in surface fluxes or tracer transport in model products.

These differences in endpoint mole fractions may develop due to the nature of how flasks were sampled during ACT-America—which spatially separated UT and LT samples—or through wind shear. Back trajectories were run at 3,000 m MSL above each LT receptor to simulate vertical profiling and no spatial separation between UT and LT samples. This test yielded statistically similar background values (Figure 8). Because the variability in the UT flask mole fractions was similar to that found by sampling model products, model smoothing was determined not a factor.

Differences in UT and LT endpoint mole fractions indicate UT-LT decoupling (Figure 8) that is likely driven by wind shear. Figure 9 shows average February 2017 CO<sub>2</sub> and CH<sub>4</sub> cross sections. Comparing mean endpoints for all-weather days, LT and UT air masses originated at approximately 47 and 37° N latitude, at altitudes of  $3,100 \pm 800$  and  $5,100 \pm 1,400$  m MSL, respectively. Thus, UT endpoint mole fractions are lower than LT ones, creating a positive bias in trace gas enhancements for the analysis below. Higher variability in UT endpoint latitudes on frontal passage flight days (also seen in simulated endpoint mole fraction variability in Figure 8) suggests increased vertical wind shear near frontal boundaries. Simulated CO<sub>2</sub> and CH<sub>4</sub> mole fractions at mean flask sample endpoint latitudes and altitudes specified above result in potential biases of  $+0.75$  ppm CO<sub>2</sub> and  $+16$  ppb CH<sub>4</sub> (LT-UT; Figure 9). These estimates fall within  $1\sigma$  of the simulated LT and UT flask sample endpoint CO<sub>2</sub> and CH<sub>4</sub> differences calculated in Figure 8 for the wintertime.

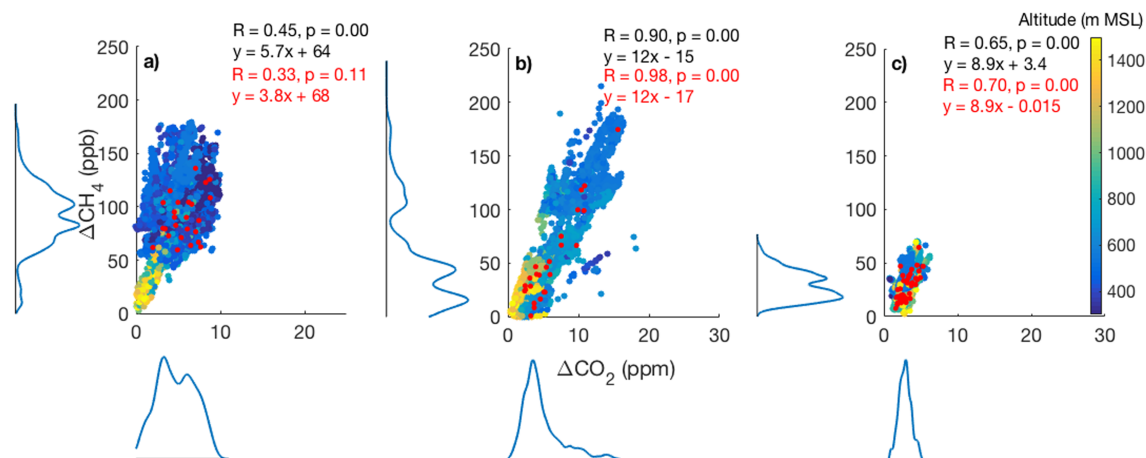


**Figure 10.**  $\text{CH}_4$  versus  $\text{CO}_2$  fair-weather LT enhancements plotted for Southeast (a), Midwest (b), and Mid-Atlantic (c) regions. Continuously measured LT enhancements are colored by altitude. Probability distribution functions of the continuous enhancements (also corrected to remove upwind vertical gradients (see section 2.5)) are shown on each axis. Black text indicates the slope and correlation from a linear least squares geometric mean regression for the continuous data, while red points and text indicate calculated flask enhancements for each region, correlations, and regressions.

During the summer, the vertical and latitudinal gradients for  $\text{CH}_4$  remain the same sign but are reversed for  $\text{CO}_2$ . NOAA/ESRL surface marine boundary layer measurements of  $\text{CO}_2$  and  $\text{CH}_4$  during February–March 2017 (<https://www.esrl.noaa.gov/gmd/ccgg/mbl/>) corroborate these model estimates in Figure 9, indicating that the latitudinal gradient between LT and UT flask endpoint mole fractions results in a +0.40 ppm  $\text{CO}_2$  and +8 ppb  $\text{CH}_4$  average bias at the surface. As discussed in section 2.6, the correction for a preexisting continental vertical gradient applied to all enhancements for species in Table 1 decreases these air mass origin biases to 0.4 ppm  $\text{CO}_2$  and 5 ppb  $\text{CH}_4$ , which results in less than a 10% bias on average for regional enhancement calculations.

### 3.2.2. Representivity of Discrete Flask Samples

With limited flask samples, we show that large-scale features are not missed and that flask samples can capture mean, regional  $\text{CO}_2$  and  $\text{CH}_4$  enhancements. Scatterplots of flask and continuous  $\Delta\text{CO}_2$  versus  $\Delta\text{CH}_4$  for each region are shown in Figure 10. Here, continuous  $\text{CO}_2$  and  $\text{CH}_4$  enhancements were calculated in the same manner as flasks (described in section 2.6). For each region, the distribution of flask  $\Delta\text{CO}_2$  and  $\Delta\text{CH}_4$  falls within the peak probability density function of continuous  $\Delta\text{CO}_2$  and  $\Delta\text{CH}_4$ . The slope and intercept of these continuous and flask scatterplots are comparable for all domains, indicating that the range of flask samples capture the mean air mass characteristics in each ACT-America region. Slightly different slopes and intercepts for flask distributions relative to continuous data are found in the Southeast due to the variability in  $\text{CO}_2$  and  $\text{CH}_4$  mole fractions observed here and to point source plumes that were outside of the normal distribution found in the majority of measurements.

### 3.3. Multispecies Assessment of $\text{CO}_2$ and $\text{CH}_4$ Enhancements

Correlation results between  $\text{CO}_2$ ,  $\text{CH}_4$ , and other source-specific trace gas species are discussed by source sector below as a qualitative approach to examine processes influencing LT  $\text{CO}_2$  and  $\text{CH}_4$  enhancements throughout the eastern United States. The implications of these results with respect to  $\text{CO}_2$  and  $\text{CH}_4$  surface sources are then discussed by each ACT-America region in section 3.4.

#### 3.3.1. Urban and Vehicular Fossil Fuel Combustion

Carbon monoxide, benzene, and acetylene are all primarily sourced from urban fossil fuel combustion and vehicular emissions (Harley et al., 1997; Warneke et al., 2007) and were used to identify  $\text{CO}_2$  and  $\text{CH}_4$  emitted from urban and vehicular fossil fuel combustion. Footprints indicated influence from urban regions in Figures 5a–5c. For the Mid-Atlantic and Midwestern regions, strong correlations between CO, benzene, and acetylene enhancements and  $\Delta\text{CO}_2$  were found that were significant at the 95% confidence interval ( $p < 0.05$ ,  $R > 0.56$ ) (Figures 11a–11c). In contrast, urban and vehicular fossil fuel tracer correlations with  $\Delta\text{CO}_2$  in the Southeast indicated almost no correlation, potentially due to the influence of wintertime ecosystem  $\text{CO}_2$  exchange on net  $\text{CO}_2$  fluxes, which will be examined in section 3.3.6. The Mid-Atlantic and the Midwest  $\Delta\text{CH}_4$  were well correlated with CO, benzene, and acetylene enhancements, suggesting  $\text{CH}_4$  variability from fossil fuel combustion (Figures 12a–12c). While significant correlations were found between

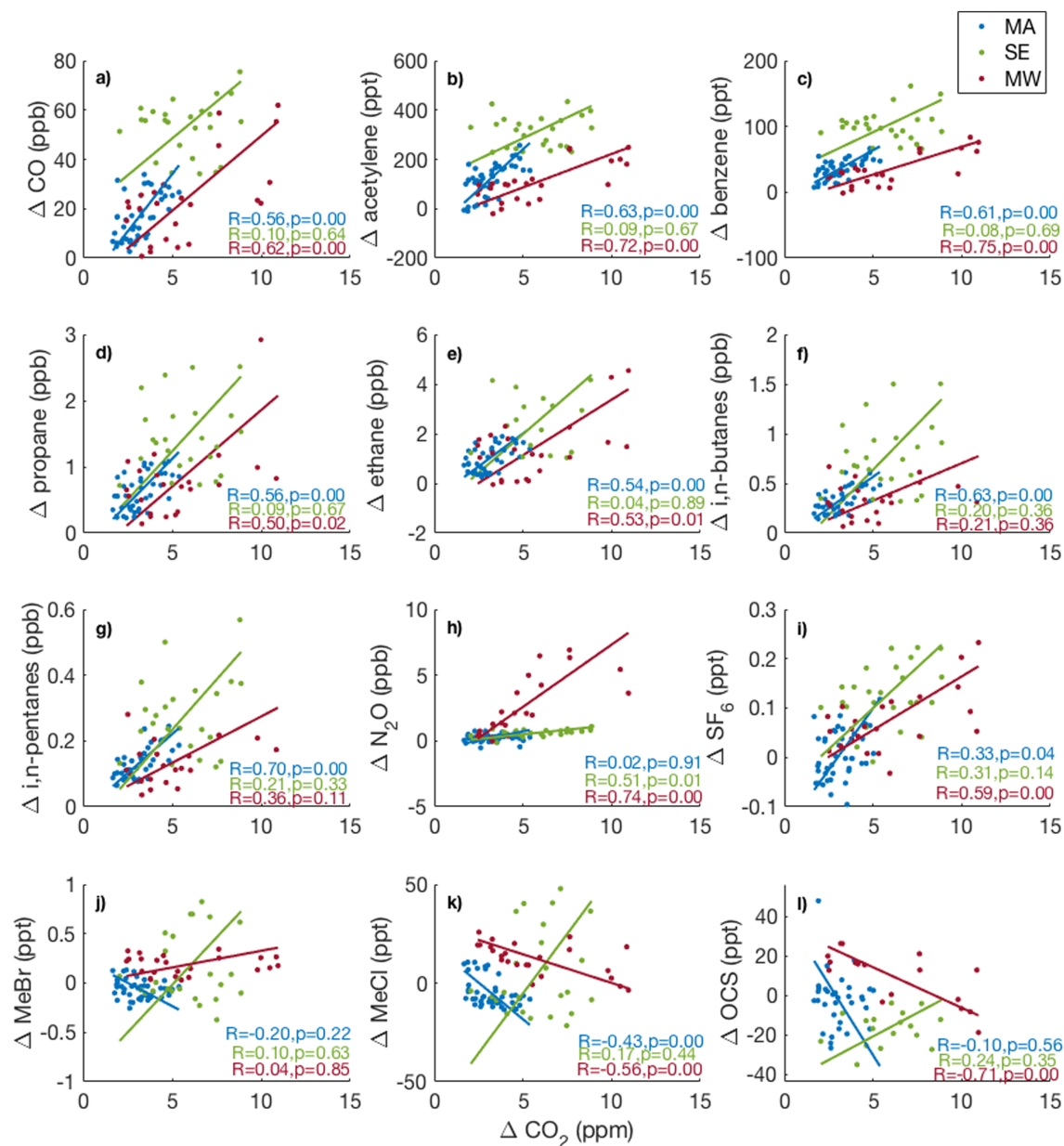


**Figure 11.** Multispecies LT (alt < 1,500 m MSL) enhancement correlations with  $\Delta \text{CO}_2$  for fair-weather flights. Enhancements are derived as in section 2.6. Points are colored by ACT-America sampling region, along with corresponding correlation coefficient ( $R$ ) and  $p$  values for correlations ( $p > 0.05$  indicates no statistically significant correlation at the 95% confidence level). Regression lines are plotted as a least squares geometric mean for the  $x$  and  $y$  axes.

$\text{CO}$ , benzene, and  $\text{CH}_4$  enhancements in the Southeast, the lack of correlation with acetylene enhancements (Figure 12b) suggests that  $\Delta \text{CH}_4$  was influenced by other, off-road combustion processes.

Due to the significant, positive correlations between  $\Delta \text{CO}$  and  $\Delta \text{CO}_2$  in the Mid-Atlantic and Midwest, we examine the slopes of these correlations compared to enhancement ratios reported in other studies. The average  $\Delta \text{CO}:\Delta \text{CO}_2$  in the Mid-Atlantic was  $9.3 \pm 1.4$  (Figure 11a), which falls outside of the range of average ratios reported for the northeastern United States during winter of 11–14 ppb  $\text{CO}:\text{ppm } \text{CO}_2$  in recent literature (Miller et al., 2012; Potosnak et al., 1999), but was within the range of  $\Delta \text{CO}:\Delta \text{CO}_2$  reported in vehicular tailpipe emissions (Ammoura et al., 2014). The observed  $\Delta \text{CO}:\Delta \text{CO}_2$  in the Midwest was  $6 \pm 1.13$  (Figure 11). Because the  $\Delta \text{CO}:\Delta \text{CO}_2$  for the Southeast was not statistically significant, it is not discussed here.

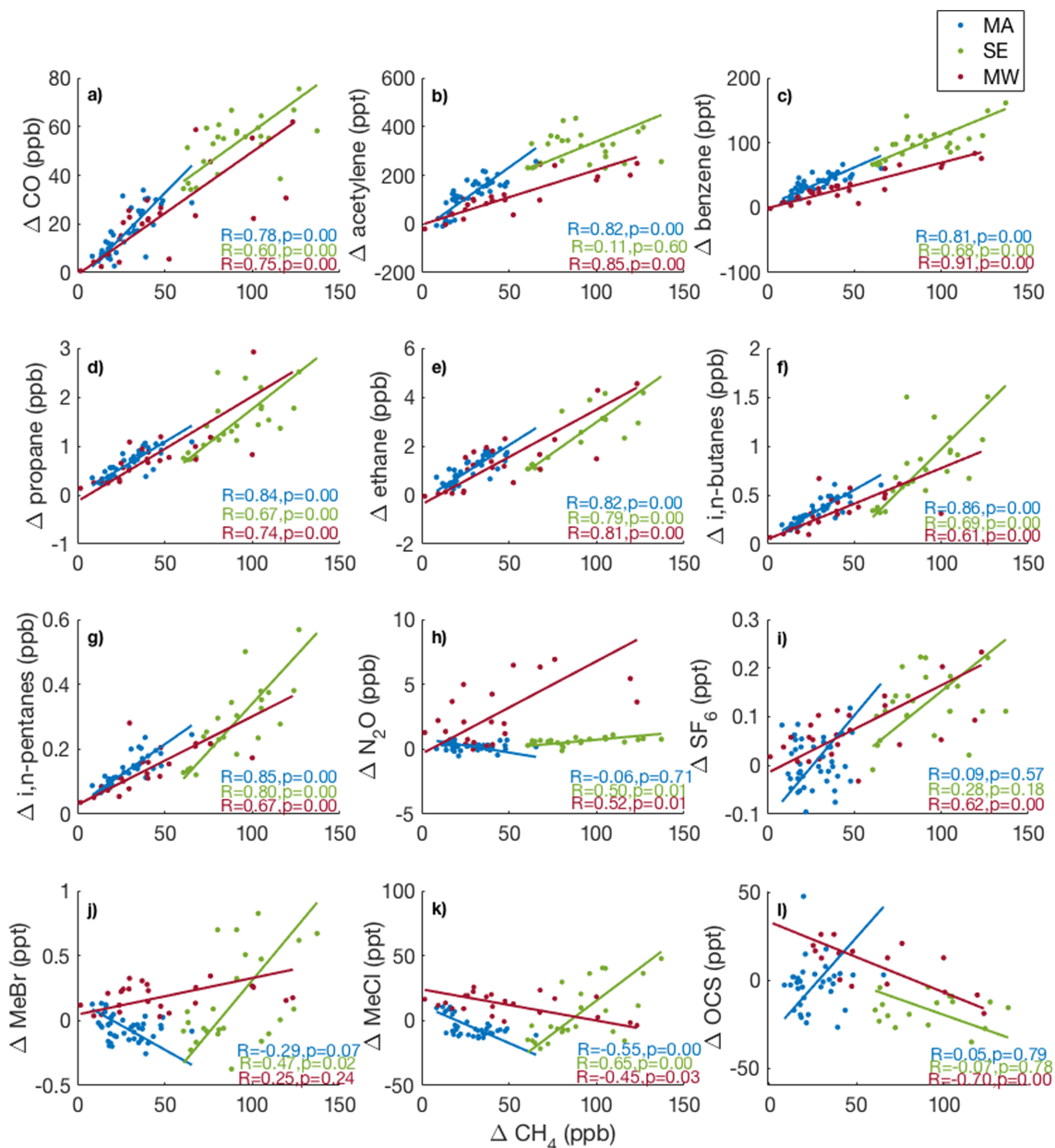


**Figure 12.** Multispecies LT (alt < 1,500 m MSL) enhancement correlations with  $\Delta\text{CH}_4$  for fair-weather flights. Enhancements are derived as in section 2.6. Points are colored by ACT-America sampling region, along with corresponding correlation coefficient ( $R$ ) and  $p$  values for correlations ( $p > 0.05$  indicates no statistically significant correlation at the 95% confidence level). Regression lines are plotted as a least squares geometric mean for the  $x$  and  $y$  axes.

### 3.3.2. Oil and Natural Gas Operations

The release of carbon from oil and natural gas operations through fossil fuel combustion or leakage is a large anthropogenic  $\text{CH}_4$  source in each region. Nonmethane hydrocarbons such as ethane and propane are primarily sourced through oil and natural gas activity (Gilman et al., 2013; Pétron et al., 2012; Swarthout et al., 2013; Thompson et al., 2014). While higher-order alkanes such as  $i,n$ -butane and  $i,n$ -pentane can be emitted from automotive fuel evaporation and the wintertime burning of fossil fuels, they are mainly derived from oil and natural gas evaporation, industrial flares, and fuel combustion (Blake & Rowland, 1986). In the Mid-Atlantic, correlations between  $\Delta\text{CO}_2$  and  $\text{C}_2$ - $\text{C}_5$  hydrocarbon enhancements were strong (Figures 11d–11g), and this region exhibited surface influence from areas encompassing both large coal and oil and natural gas operations (Figure 5c) (Barkley et al., 2017). In the Midwest, strong correlations were also found between  $\Delta\text{CO}_2$ ,  $\Delta$ ethane and  $\Delta$ propane (Figures 11d and 11e), but not higher-order alkanes such

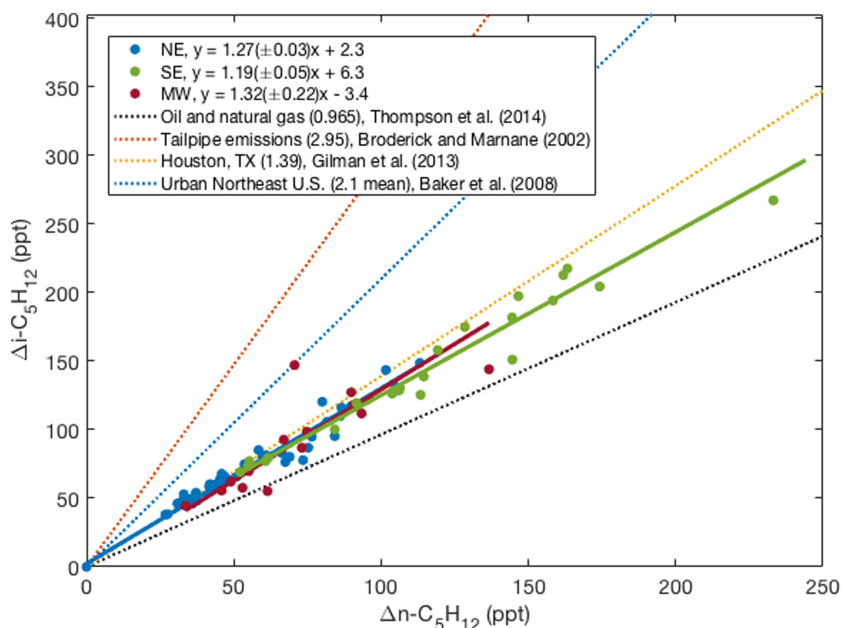


**Figure 13.** Regional LT  $\Delta i$ -pentane: $\Delta n$ -pentane ratios for fair-weather flights. Ratios are indicated by slopes ( $\pm 1\sigma$ ) of linear least squares bisector regressions for each color-coded region. Slopes of  $i:n$ -pentane ratios of other regions within the United States are also denoted for comparison. Slopes derived from  $\Delta i$ -pentane: $\Delta n$ -pentane were not significantly different from those derived from lower-tropospheric  $i:n$ -pentane mole fractions, indicating that the source signature of continental background air does not significantly affect these results.

as pentanes and butanes. In the Southeastern region, no significant correlations between  $\Delta\text{CO}_2$  and  $\text{C}_2$ - $\text{C}_5$  hydrocarbon enhancements were found, similar to correlations observed with urban and vehicular fossil fuel tracers. For all three domains,  $\Delta\text{CH}_4$  were well correlated with ethane and propane enhancements ( $R > 0.67$ ; Figures 12d–12e).

The ratio of  $\Delta i$ -pentane: $\Delta n$ -pentane can inform the relative influence of the oil and natural gas emissions versus urban or vehicular emissions (Figure 13). Recent literature reports this ratio to be 2–3 for urban areas and tailpipe emissions and  $\sim 1$  or lower in oil- and natural gas-influenced areas (Baker et al., 2008; Broderick & Marnane, 2002; Gilman et al., 2013; Thompson et al., 2014); all ACT-America regions exhibited an average  $i:n$ -pentane ratio of 1.3, with no significant differences observed between the three study regions. Regional footprints also indicate surface influence near large oil and natural gas shale plays (Figure 5). Further, the  $\Delta\text{ethane}:\Delta\text{CH}_4$  ratio observed in the Mid-Atlantic and Southeastern United States is comparable to other enhancement ratios reported in recent literature. This enhancement ratio for the Mid-Atlantic was 4.5% (Figure 12e): within the range of reported ratios for Mid-Atlantic region shale plays (Marcellus, Utica) of 2–16% (Conder & Lawlor, 2014; Peischl et al., 2015) and higher than the reported 2.6–3.3%  $\Delta\text{ethane}:\Delta\text{CH}_4$  in dense urban regions (Plant et al., 2019). In the Southeast, this enhancement ratio was approximately 5% (Figure 12e), which is within the range of 2–10% reported in both Smith et al. (2015) and Peischl et al. (2018) for the Bakken and other shale plays in this region. The Midwest  $\Delta\text{ethane}:\Delta\text{CH}_4$  was 3.8% (Figure 12e), lower than those reported in the Bakken shale formation and Denver basins (approximately 50% and 16%, respectively; Peischl et al., 2018). This lower ratio is likely due to agricultural emissions (Figure 5b) but still generally higher than that found in urban areas.

### 3.3.3. Agriculture

Bottom-up inventories suggest that agriculture is the main source of  $\text{CH}_4$  and anthropogenic nitrous oxide ( $\text{N}_2\text{O}$ ) emissions in the Midwestern United States (US EPA, 2016). Over half of the U.S. anthropogenic  $\text{N}_2\text{O}$  emissions are attributed to agriculture (Bouwman et al., 1995; Davidson & Kanter, 2014), and small amounts of  $\text{N}_2\text{O}$  can be emitted from fossil fuel combustion (Becker et al., 2000). In the Mid-Atlantic, no significant correlations between  $\Delta\text{CO}_2$  and  $\Delta\text{N}_2\text{O}$  were found. Correlations between  $\Delta\text{N}_2\text{O}$  and  $\Delta\text{CO}_2$  yielded  $R$  values of 0.74 and 0.51 in the Midwest and Southeast regions, respectively (Figure 11h). The  $\Delta\text{N}_2\text{O}$  was not well correlated with other urban tracers in this region, further suggesting ecosystem sources of  $\text{CO}_2$ .

Midwest  $\Delta\text{N}_2\text{O}$  were approximately five times the  $\Delta\text{N}_2\text{O}$  in the Mid-Atlantic and Southeast and were correlated to  $\Delta\text{CH}_4$  and  $\Delta\text{N}_2\text{O}$  (Figure 12h). In the Southeast, where large agricultural  $\text{CH}_4$  emissions are prevalent (Maasakkers et al., 2016), strong correlations between  $\Delta\text{CH}_4$  and  $\Delta\text{N}_2\text{O}$  were also observed.

### 3.3.4. Energy Transmission

Sulfur hexafluoride ( $\text{SF}_6$ ) is primarily used as a dielectric within the electricity sector, escaping into the atmosphere through leaks and venting (Ko et al., 1993; Olivier et al., 2005). Given its long atmospheric lifetime ( $\sim 850$  years), and typical colocated emissions with  $\text{CO}_2$  and  $\text{CH}_4$  from fossil fuel-powered energy facilities,  $\text{SF}_6$  is examined as a tracer for coal-fired and natural gas-fired power plant emissions of  $\text{CO}_2$  and  $\text{CH}_4$ , respectively. For the Mid-Atlantic and Midwest, statistically significant ( $p < 0.05$ ) correlations between  $\Delta\text{SF}_6$  and  $\Delta\text{CO}_2$  were found. No significant correlation was found in the Southeast between  $\Delta\text{CO}_2$  and  $\Delta\text{SF}_6$  (Figure 11i). Higher  $\text{SF}_6$  and  $\text{CO}_2$  and  $\text{CH}_4$  correlations resulting from colocated emissions from the energy sector could be expected in high-density population regions in the absence of other, significant sources. In this analysis, significant correlations between  $\Delta\text{SF}_6$  and  $\Delta\text{CO}_2$  and  $\Delta\text{CH}_4$  are only found in the Midwest (Figure 11i, Figure 12i). Emissions of  $\text{SF}_6$  are sporadic and based on energy usage, with energy generation, transmission, and distribution facilities acting as a single point source. Closer to emissions sources, high correlations between  $\Delta\text{SF}_6$ ,  $\Delta\text{CO}_2$ , and  $\Delta\text{CH}_4$  are expected; however, on regional scales, lower correlations are observed. Thus, the higher variability between  $\Delta\text{SF}_6$ ,  $\Delta\text{CO}_2$ , and  $\Delta\text{CH}_4$  correlations observed at these regional spatial scales is expected.

### 3.3.5. Wetlands and Biomass Burning

Methyl halides (i.e., methyl chloride ( $\text{MeCl}$ ) and methyl bromide ( $\text{MeBr}$ )) have large natural emissions sources including oceans, coastal salt marshes and wetlands, soils, and other plants (Khalil et al., 1998; Rhew et al., 2000; Varner, 1999). Anthropogenic sources of  $\text{MeCl}$  include biomass burning (Crutzen et al., 1979; Lobert et al., 1999), with enhanced natural emissions in coastal regions due to chlorine deposition derived from sea salt. While  $\text{MeBr}$  also has other anthropogenic emissions sources, these are likely small relative to natural emissions due to their phaseout by the Montreal Protocol (United Nations Environment Programme, 2019).

In the Mid-Atlantic and Midwest, methyl halide enhancements exhibited a negative correlation with  $\Delta\text{CO}_2$  and  $\Delta\text{CH}_4$  (Figures 12j and 12k, Figures 11j and 11k). As sinks of methyl halides include a small loss to the ocean and microbial degradation in soils (Keppler et al., 2005; Serça et al., 1998), depletions in methyl halides relative to the UT continental background were observed in the Mid-Atlantic and Southeast. However, some of the largest depletions in methyl halides were observed in the Southeast, alongside positive correlations with  $\Delta\text{CO}_2$  and  $\Delta\text{CH}_4$ .

In contrast, methyl halide enhancements in the Southeast were high during 9–10 February 2017 relative to all other campaign flight days. During this period, positive correlations were observed between  $\Delta\text{MeCl}$  and  $\Delta\text{CO}_2$  but were statistically insignificant. Statistically significant positive  $\Delta\text{CH}_4$  correlations with methyl halide enhancements were found in the Southeast, with  $\Delta\text{CH}_4$  greater than 100 ppb and other coenhanced species such as  $\text{C}_3$ - $\text{C}_5$  hydrocarbons, carbonyl sulfide, and ozone.

### 3.3.6. Biogenic Uptake

Carbonyl sulfide ( $\text{OCS}$ ) seasonality in the Northern Hemisphere is largely driven by plant photosynthetic uptake in a manner similar to  $\text{CO}_2$  (Montzka et al., 2007).  $\text{OCS}$  is also emitted in small amounts through anthropogenic activity, particularly from cold-running vehicular emissions (Fried et al., 1992). During winter 2017, a negative correlation between  $\Delta\text{OCS}$  and  $\Delta\text{CO}_2$  was found in the Mid-Atlantic and Midwest regions. As discussed above, soil uptake of methyl halides is most evident in the Southeast from observed depletions of tracer mole fractions relative to the UT. Molecular hydrogen (not shown) also has a large sink due to soil uptake (Novelli et al., 1999) and shows the largest depletions in the Southeast, and a positive correlation to  $\Delta\text{CO}_2$ . Similar to these biogenic tracers, the lowest average  $\Delta\text{OCS}$  was observed in the Southeast (Figure 11l). The positive  $\Delta\text{OCS}$ - $\Delta\text{CO}_2$  correlation in the Southeast is in contrast to the  $\Delta\text{OCS}$ - $\Delta\text{CO}_2$  correlation in other regions. A weak correlation between  $\text{OCS}$  and other vehicular fossil fuel combustion tracers such as  $\text{CO}$ , benzene, and acetylene in the Southeast suggests that vehicular emissions are not a significant source of  $\text{OCS}$  influencing this regression.

## 3.4. Discussion

Examining tracer enhancements concurrently with  $\Delta\text{CO}_2$  and  $\Delta\text{CH}_4$  can help to illuminate significant anthropogenic and biogenic processes that influence  $\Delta\text{CO}_2$  and  $\Delta\text{CH}_4$  variability in each of the three

ACT-America study regions. However, few species measured in flasks are source specific; here, we discuss significant correlations to source tracers, enhancement ratios, and implications for CO<sub>2</sub> and CH<sub>4</sub> sources.

#### 3.4.1. Mid-Atlantic

Figure 10 indicates that Mid-Atlantic  $\Delta\text{CO}_2$  and  $\Delta\text{CH}_4$  were smaller than the other study regions during winter 2017. Higher wind speeds in the Mid-Atlantic during February–March 2017 greatly diluted enhancement signals, yielding lower surface influence in Figure 5 than in other ACT-America regions despite large known urban and vehicular fossil fuel combustion and oil and natural gas emissions. Carbon enhancements from flasks sampled off of the coast of Cape May, NJ, from 2011 to 2017 (“CMA,” Figure 2) in the NOAA CCGG small aircraft network show larger climatological wintertime  $\Delta\text{CO}_2$  and  $\Delta\text{CH}_4$  than that observed during the ACT-America campaign, also indicating that the ACT-America sampling time period experienced anomalous wintertime meteorological conditions.

Both  $\Delta\text{CO}_2$  and  $\Delta\text{CH}_4$  were strongly correlated in the Mid-Atlantic ( $R = 0.70$ , Figure 10c) and exhibited significant, positive correlations to urban and oil and natural gas tracer (CO, acetylene, benzene, propane, ethane, butanes, and pentanes) enhancements. Thus, anthropogenic, fossil fuel combustion sources dominated observed  $\Delta\text{CO}_2$  and  $\Delta\text{CH}_4$  variability in this region. Vehicular-dominated sources were not apparent in Figures 11a–11c because flight patterns were generally concentrated near oil and gas production regions rather than urban regions (Figure 5c). The observed Mid-Atlantic  $\Delta\text{CO}:\Delta\text{CO}_2$  ratio for this region indicates relatively efficient combustion (in contrast to less efficient biomass burning) and was slightly lower than ratios reported in the studies above. As the  $\Delta i:n$ -pentane ratio indicates oil and natural gas-influenced combustion sources, these ratios represent a mixture of both vehicular and nonvehicular fossil fuel point source types. This average enhancement ratio of 9.3 assumes that all of the  $\Delta\text{CO}_2$  can be attributed to fossil fuel combustion sources; however, without analysis of the radiocarbon content ( $\Delta^{14}\text{CO}_2$ ) of CO<sub>2</sub>, the above ratio can include nonfossil fuel sources. Nonfossil fuel sources are expected to be small, and the average correlation ( $R = 0.60$ ) between  $\Delta\text{CO}_2$  and tracers in Figures 11a–11g indicates that the majority of  $\Delta\text{CO}_2$  variability is anthropogenic. Using  $\Delta^{14}\text{CO}_2$ , Miller et al. (2012) found that up to 50% of the total CO<sub>2</sub> signal could be attributed to ecosystem respiration during the wintertime in the northeastern United States. As such, depletions in methyl halides do indicate some ecosystem processing in Figure 11.

$\Delta\text{CH}_4$  was strongly correlated with ethane, propane, and higher-order alkane enhancements that are all primarily sourced from the oil and natural gas industry. Fossil fuel combustion tracer enhancements thereby explain approximately 80% of the variability in  $\Delta\text{CH}_4$  for this study. The examination of ratios between  $i$ - and  $n$ -pentane isomers was slightly lower than those reported from northeastern U.S. cities, which are within the range of 1.4 to 2.8 (Baker et al., 2008), further indicating that  $\Delta\text{CH}_4$  variability had a nonnegligible influence from the oil and natural gas industry.

#### 3.4.2. Midwest

Similar to the Mid-Atlantic region, statistically significant Midwestern  $\Delta\text{CO}_2$  correlations with urban/vehicular and oil and natural gas tracer enhancements suggest that the variability in  $\Delta\text{CO}_2$  is largely explained by anthropogenic fossil fuel combustion sources. Conversely, strong correlations between  $\Delta\text{N}_2\text{O}$  and  $\Delta\text{CO}_2$  may be an effect of colocated sources of agricultural N<sub>2</sub>O and ecosystem CO<sub>2</sub> respiration. Both soil N<sub>2</sub>O (Mosier, 1998; Shepherd et al., 1991) and ecosystem respiration (CO<sub>2</sub> effluxes) are temperature dependent, and surface temperatures for the Midwestern domain during this flight campaign were above 21° C at times, reaching record highs. Thus, these higher-than-average temperatures may be one cause of large wintertime enhancements in N<sub>2</sub>O and the strong correlation to  $\Delta\text{CO}_2$ . The  $\Delta\text{CO}:\Delta\text{CO}_2$  observed in the Midwest is lower than typical reported vehicular  $\Delta\text{CO}:\Delta\text{CO}_2$  ratios, further reflecting a mixture of nonanthropogenic and anthropogenic point sources in this region (Figure 5b).

The correlation between  $\Delta\text{CO}_2$  and  $\Delta\text{CH}_4$  ( $R = 0.98$ , Figure 10b) also suggests that CO<sub>2</sub> and CH<sub>4</sub> sources may be colocated. The predominance of agriculture in this region is indicated by the large fraction of the variability in  $\Delta\text{CH}_4$  associated with  $\Delta\text{N}_2\text{O}$  (Figure 12h). Strong correlations between  $\Delta\text{CH}_4$  and anthropogenic tracer enhancements (CO, benzene, acetylene, and C<sub>2</sub>–C<sub>6</sub> hydrocarbons; Figures 12a–12g) were observed in the Midwestern study region indicating that variability in  $\Delta\text{CO}_2$  and  $\Delta\text{CH}_4$  is largely dominated by anthropogenically sourced tracers.

#### 3.4.3. Southeast

Potential biological uptake and ecosystem respiration was found to create additional variability in observed  $\Delta\text{CO}_2$  correlations. In addition, remote sensing phenology records indicate that Southeast vegetation is more active by February than the other study regions (USGS, 2019). Consequently, weak and/or statistically

insignificant correlations between  $\Delta\text{CO}_2$  and  $\Delta\text{CH}_4$  (Figure 10a) and between  $\Delta\text{CO}_2$  other anthropogenic tracers in the Southeast is indicative of the influence of ecosystem  $\text{CO}_2$  exchange, similar to  $\Delta\text{CO}_2$  correlations observed in Miller et al. (2012). While  $\Delta\text{OCS}$  can provide some clues into  $\Delta\text{CO}_2$  variability due to biological uptake, its correlation to  $\Delta\text{CO}_2$  was insignificant. However, the positive correlation between  $\Delta\text{OCS}$  and  $\Delta\text{CO}_2$  in contrast to negative Midwest and Mid-Atlantic correlations suggests that biogenic uptake of  $\text{CO}_2$  contributes to the net  $\text{CO}_2$  flux for the Southeast during winter. Given known anthropogenic sources of  $\text{CO}_2$  in this region, their contribution to  $\Delta\text{CO}_2$  variability may be masked in many correlations to  $\Delta\text{CO}_2$  due to wintertime biogenic  $\text{CO}_2$  uptake. Although soil uptake processes are different from photosynthesis, the depletion of other biogenic tracers (methyl halides, hydrogen) in the Southeast is further indicative of active wintertime ecosystem processing.

Significant correlations between  $\Delta\text{CH}_4$  and both anthropogenic and biogenic tracers are also found. Methyl chloride enhancements in particular explain over 40% of the  $\Delta\text{CH}_4$  variability. Wetland emissions can be one source for methyl halides; they can also be emitted from biomass burning in the Southeast during winter mainly from prescribed, residential, and agricultural burning (Liu et al., 2016; Tian et al., 2009; Zhang et al., 2010). Observed enhancements in methyl halide and other nonmethane hydrocarbons alongside multiple fire counts remotely observed from the NASA Visible Infrared Imaging Radiometer Suite (VIIRS) (NASA, 2018) near flight paths between 9–10 February 2017 support biomass burning as one source of methyl halide and  $\text{CH}_4$  enhancement variability in the Southeast. As footprints in Figure 5a also intersect large wetland regions,  $\Delta\text{CH}_4$  variability may also be influenced by wetland emissions during these events. Due to the potential colocation of biomass burning and wetland sources, it is difficult to disaggregate the two without the use of additional tracers.

#### 4. Summary and Conclusions

Regional  $\text{CO}_2$  and  $\text{CH}_4$  enhancements during the winter 2017 ACT-America campaign were computed using multispecies measurements in aircraft flasks sampled under fair weather conditions. We use background mole fractions from the UT, hypothesizing that the use of upper-atmospheric observations to define background is more appropriate during winter due to decreased wind shear, and to decreased convective mixing of surface emissions into the upper atmosphere. Model products were used as a realistic test environment alongside aircraft and surface observations for understanding potential issues with estimating background mole fractions for this analysis.

Correlations between  $\Delta\text{CO}_2$ ,  $\Delta\text{CH}_4$  and fossil fuel combustion tracers,  $\Delta\text{ethane}:\Delta\text{CH}_4$ , and  $\Delta\text{i:n-pentane}$  all indicate that the variability in  $\Delta\text{CO}_2$  and  $\Delta\text{CH}_4$  in the all regions was broadly influenced by oil and natural gas emissions and that most enhancements were anthropogenically sourced. Mid-Atlantic oil and natural gas sources were evident as a result of close sampling proximity to dense oil and natural gas wells. Large nitrous oxide enhancements in the Midwest alongside  $\Delta\text{CO}_2$  under anomalously high temperatures highlight prevalent agricultural sources and potential  $\text{CO}_2$  respiration. Wintertime biogenic uptake of  $\text{CO}_2$  emerged as a source of  $\Delta\text{CO}_2$  variability in the Southeast, complicating  $\Delta\text{CO}_2$  and anthropogenic tracer enhancement correlations in the absence of  $^{14}\text{CO}_2$  measurements. However, the aggregate of fossil fuel, wetland  $\text{CH}_4$  sources, and biomass burning sources in the Southeast contributed to large surface  $\text{CH}_4$  enhancements during the wintertime.

We show that flask sampling can indicate major sources of  $\text{CO}_2$  and  $\text{CH}_4$  enhancement variability for informing regional-scale  $\text{CO}_2$  and  $\text{CH}_4$  flux priors. However, this analysis also highlights limitations in these measurements. Sparse sampling near source regions and lack of a more diverse suite of source-specific tracers inhibits quantitative source attribution. The mixture of emissions source types and tracer-tracer ratios over large sample regions makes using a single tracer (other than  $^{14}\text{CO}_2$ ) for this analysis difficult. Quantitatively attributing  $\Delta\text{CO}_2$  and  $\Delta\text{CH}_4$  to specific source sectors will require (a) increasing sampling nearer to sources to isolate and increase enhancement signals over background levels and (b) the inclusion of more uniquely sourced tracers either in or alongside the flask measurement suite. Additional species could include nitrogen oxides as an urban tracer (Goldan et al., 2012); biomass burning tracers, acetonitrile, aerosols, and  $\text{C}_3\text{-C}_4$  alkynes (Andreae & Merlet, 2001; Blake et al., 1996); and ammonia as an agricultural tracer (Anderson et al., 2003). While  $^{14}\text{CO}_2$  sampling is limited during the ACT-America campaign, its use for partitioning  $\Delta\text{CO}_2$  into fossil fuel and biogenic components can also enhance  $\text{CO}_2$  source attribution analyses.

**Acknowledgments**

ACT-America is a NASA Earth Venture Suborbital 2 project funded by NASA's Earth Science Division. The authors acknowledge support from this division for Grant NNX15AJ06G to the University of Colorado and Grant NNX15AG76G to the Pennsylvania State University. We gratefully thank the following NOAA/ESRL/GMD colleagues who have handled or made measurements in flasks in support of this campaign: P. Lang, E. Moglia, C. Siso, M. Crotwell, A. Crotwell, B. Hall, D. Neff, S. Wolter, and J. Kofler. We thank the ACT-America scientific and administrative team members for their valuable support during the ACT-America field missions. We acknowledge the NOAA Air Resources Laboratory (ARL) for the provision of the HYSPLIT dispersion model. NOAA CarbonTracker CT-NRT.v2018-1 results are provided by NOAA ESRL, Boulder, Colorado, USA (from the website at <http://carbontracker.noaa.gov>). The authors declare, to their knowledge, no conflicts of interest with the submittal of this manuscript. All ACT-America flask and in situ data used in this manuscript can be found online (at <https://doi.org/10.3334/ORNLDAAC/1593>).

**References**

Ammoura, L., Xueref-Remy, I., Gros, V., Baudic, A., Bonsang, B., Petit, J.-E., et al. (2014). Atmospheric measurements of ratios between CO<sub>2</sub> and co-emitted species from traffic: a tunnel study in the Paris megacity. *Atmospheric Chemistry and Physics*, *14*(23), 12,871–12,882. <https://doi.org/10.5194/acp-14-12871-2014>

Anderson, N., Strader, R., & Davidson, C. (2003). Airborne reduced nitrogen: ammonia emissions from agriculture and other sources. *Environment International*, *29*(2), 277–286. [https://doi.org/10.1016/S0160-4120\(02\)00186-1](https://doi.org/10.1016/S0160-4120(02)00186-1)

Andreae, M. O., & Merlet, P. (2001). Emission of trace gases and aerosols from biomass burning, global biogeochem. *Cycles*, *15*(4), 955–966. <https://doi.org/10.1029/2000GB001382>

Baker, A. K., Beyersdorf, A. J., Doezema, L. A., Katzenstein, A., Meinardi, S., Simpson, J. I., et al. (2008). Measurements of nonmethane hydrocarbons in 28 United States cities. *Atmospheric Environment*, *42*(1), 170–182. <https://doi.org/10.1016/j.atmosenv.2007.09.007>

Baker, D. F., Law, R. M., Gurney, K. R., Rayner, P., Peylin, P., Denning, A. S., et al. (2006). TransCom 3 inversion intercomparison: Impact of transport model errors on the interannual variability of regional CO<sub>2</sub> fluxes, 1988–2003. *Global Biogeochemical Cycles*, *20*, GB1002. <https://doi.org/10.1029/2004GB002439>

Barkley, Z. R., Lauvaux, T., Davis, K. J., Deng, A., Miles, N. L., Richardson, S. J., et al. (2017). Quantifying methane emissions from natural gas production in north-eastern Pennsylvania. *Atmospheric Chemistry and Physics*, *17*(22), 13,941–13,966. <https://doi.org/10.5194/acp-17-13941-2017>

Becker, K. H., Lörzer, J. C., Kurtenbach, R., Wiesen, P., Jensen, T. E., & Wallington, T. J. (2000). Contribution of vehicle exhaust to the global N<sub>2</sub>o budget. *Chemosphere - Global Change Science*, *2*(3), 387–395. [https://doi.org/10.1016/S1465-9972\(00\)00017-9](https://doi.org/10.1016/S1465-9972(00)00017-9)

Birdsey, R., Mayes, M., Najjar, R., Reed, S., Romero-Lankao, P., & Zhu, Z. e. (2018). Second State of the Carbon Cycle Report (SOCCR2): A Sustained Assessment Report (U.S. Global Change Research Program SOCCR2 Report). Washington, DC, USA: U.S. Global Change Research Program.

Blake, N. J., Blake, D. R., Sive, B. C., Chen, T.-Y., Rowland, F. S., Collins, J. E., et al. (1996). Biomass burning emissions and vertical distribution of atmospheric methyl halides and other reduced carbon gases in the South Atlantic region. *Journal of Geophysical Research*, *101*(D19), 24,151–24,164. <https://doi.org/10.1029/96JD00561>

Blake, N. J., Campbell, J. E., Vay, S. A., Fuelberg, H. E., Huey, L. G., Sachse, G., et al. (2008). Carbonyl sulfide (OCS): Large-scale distributions over North America during INTEX-NA and relationship to CO<sub>2</sub>. *Journal of Geophysical Research*, *113*, D09S90. <https://doi.org/10.1029/2007JD009163>

Blake, D. R., & Rowland, F. S. (1986). World-wide increase in tropospheric methane, 1978–1983. *Journal of Atmospheric Chemistry*, *4*(1), 43–62. <https://doi.org/10.1007/BF00053772>

Born, M., Dörr, H., & Levin, I. (1990). Methane consumption in aerated soils of the temperate zone. *Tellus B*, *42*(1), 2–8. <https://doi.org/10.1034/j.1600-0889.1990.00002.x>

Bousquet, P., Ciais, P., Peylin, P., Ramonet, M., & Monfray, P. (1999). Inverse modeling of annual atmospheric CO<sub>2</sub> sources and sinks: 1. Method and control inversion. *Journal of Geophysical Research*, *104*(D21), 26,161–26,178. <https://doi.org/10.1029/1999JD900342>

Bousquet, P., Peylin, P., Ciais, P., Quére, C. L., Friedlingstein, P., & Tans, P. P. (2000). Regional changes in carbon dioxide fluxes of land and oceans since 1980. *Science*, *290*(5495), 1342–1346. <https://doi.org/10.1126/science.290.5495.1342>

Bouwman, A. F., Hoek, K. W. V. d., & Olivier, J. G. J. (1995). Uncertainties in the global source distribution of nitrous oxide. *Journal of Geophysical Research*, *100*(D2), 2785–2800. <https://doi.org/10.1029/94JD02946>

Brandt, A. R., Heath, G. A., Kort, E. A., O'Sullivan, F., Petron, G., Jordaan, S. M., et al. (2014). Methane leaks from North American natural gas systems. *Science*, *343*(6172), 733–735. <https://doi.org/10.1126/science.1247045>

Broderick, B., & Marnane, I. (2002). A comparison of the C<sub>2</sub>-C<sub>9</sub> hydrocarbon compositions of vehicle fuels and urban air in Dublin, Ireland. *Atmospheric Environment*, *36*(6), 975–986. [https://doi.org/10.1016/S1352-2310\(01\)00472-1](https://doi.org/10.1016/S1352-2310(01)00472-1)

Cambaliza, M. O. L., Shepson, P. B., Bogner, J., Caulton, D. R., Stirn, B., Sweeney, C., et al. (2015). Quantification and source apportionment of the methane emission flux from the city of Indianapolis. *Elementa: Science of the Anthropocene*, *3*, 000037. <https://doi.org/10.12952/journal.elementa.000037>

Cambaliza, M. O. L., Shepson, P. B., Caulton, D. R., Stirn, B., Samarov, D., Gurney, K. R., et al. (2014). Assessment of uncertainties of an aircraft-based mass balance approach for quantifying urban greenhouse gas emissions. *Atmospheric Chemistry and Physics*, *14*(17), 9029–9050. <https://doi.org/10.5194/acp-14-9029-2014>

Chang, R. Y.-W., Miller, C. E., Dinardo, S. J., Karion, A., Sweeney, C., Daube, B. C., et al. (2014). Methane emissions from Alaska in 2012 from CARVE airborne observations. *Proceedings of the National Academy of Sciences of the United States of America*, *111*(47), 16,694–16,699. <https://doi.org/10.1073/pnas.1412953111>

Chevallier, F., Ciais, P., Conway, T. J., Aalto, T., Anderson, B. E., Bousquet, P., et al. (2010). CO<sub>2</sub> Surface fluxes at grid point scale estimated from a global 21 year reanalysis of atmospheric measurements. *Journal of Geophysical Research*, *115*, D21307. <https://doi.org/10.1029/2010JD013887>

Choi, Y., Vay, S. A., Vadrevu, K. P., Soja, A. J., Woo, J.-H., Nolf, S. R., et al. (2008). Characteristics of the atmospheric CO<sub>2</sub> signal as observed over the conterminous United States during INTEX-NA. *Journal of Geophysical Research*, *113*, D07301. <https://doi.org/10.1029/2007JD008899>

Ciais, P., Rayner, P., Chevallier, F., Bousquet, P., Logan, M., Peylin, P., & Ramonet, M. (2010). Atmospheric inversions for estimating CO<sub>2</sub> fluxes: methods and perspectives. *Climatic Change*, *103*(1–2), 69–92. <https://doi.org/10.1007/s10584-010-9909-3>

Ciais, P., Sabine, C., Bala, G., Bopp, L., Brovkin, V., Canadell, J., et al. (2014). Carbon and other biogeochemical cycles. *Climate change 2013: The physical science basis. Contribution of Working Group I to the Fifth Assessment Report of the Intergovernmental Panel on Climate Change* (pp. 465–570). Cambridge: Cambridge University Press.

Conder, M., & Lawlor, K. (2014). Production characteristics of liquids-rich resource plays challenge facility design. accessed November 11, 2019.

Crutzen, P. J., Heidt, L. E., Krasnec, J. P., Pollock, W. H., & Seiler, W. (1979). Biomass burning as a source of atmospheric gases CO, H<sub>2</sub>, N<sub>2</sub>o, CH<sub>3</sub>CL and COS. *Nature*, *282*(5736), 253. <https://doi.org/10.1038/282253a0>

Davidson, E. A., & Kanter, D. (2014). Inventories and scenarios of nitrous oxide emissions. *Environmental Research Letters*, *9*(10), 105012. <https://doi.org/10.1088/1748-9326/9/10/105012>

Diaz-Isaac, L. I., Lauvaux, T., & Davis, K. J. (2018). Impact of physical parameterizations and initial conditions on simulated atmospheric transport and CO<sub>2</sub> mole fractions in the US Midwest. *Atmospheric Chemistry and Physics Discussions*, *18*, 14,813–14,835. <https://doi.org/10.5194/acp-2018-117>

- Dlugokencky, E. J., Myers, R. C., Lang, P. M., Masarie, K. A., Crotwell, A. M., Thoning, K. W., et al. (2005). Conversion of NOAA atmospheric dry air CH<sub>4</sub> mole fractions to a gravimetrically prepared standard scale. *Journal of Geophysical Research*, *110*, D18306. <https://doi.org/10.1029/2005JD006035>
- Dlugokencky, E. J., Steele, L. P., Lang, P. M., & Masarie, K. A. (1994). The growth rate and distribution of atmospheric methane. *Journal of Geophysical Research*, *99*(D8), 17,021–17,043. <https://doi.org/10.1029/94JD01245>
- Draxler, R. R., & Hess, G. D. (1997). Description of the HYSPLIT4 modeling system.
- Francey, R. J., Tans, P. P., Allison, C. E., Enting, I. G., White, J. W. C., & Trolier, M. (1995). Changes in oceanic and terrestrial carbon uptake since 1982. *Nature*, *373*, 326.
- Fried, A., Henry, B., Ragazzi, R. A., Merrick, M., Stokes, J., Pyzdrowski, T., & Sams, R. (1992). Measurements of carbonyl sulfide in automotive emissions and an assessment of its importance to the global sulfur cycle. *Journal of Geophysical Research*, *97*(D13), 14,621–14,634. <https://doi.org/10.1029/92JD01358>
- Gerbig, C., Lin, J. C., Wofsy, S. C., Daube, B. C., Andrews, A. E., Stephens, B. B., et al. (2003). Toward constraining regional-scale fluxes of CO<sub>2</sub> with atmospheric observations over a continent: 1. Observed spatial variability from airborne platforms. *Journal of Geophysical Research*, *108*(D24), 4756. <https://doi.org/10.1029/2002JD003018>
- Gilman, J. B., Lerner, B. M., Kuster, W. C., & de Gouw, J. A. (2013). Source signature of volatile organic compounds from oil and natural gas operations in northeastern Colorado. *Environmental Science & Technology*, *47*(3), 1297–1305. <https://doi.org/10.1021/es304119a>
- Gloor, M., Fan, S.-M., Pacala, S., & Sarmiento, J. (2000). Optimal sampling of the atmosphere for purpose of inverse modeling: A model study. *Global Biogeochemical Cycles*, *14*(1), 407–428. <https://doi.org/10.1029/1999GB900052>
- Göckede, M., Michalak, A. M., Vickers, D., Turner, D. P., & Law, B. E. (2010). Atmospheric inverse modeling to constrain regional-scale CO<sub>2</sub> budgets at high spatial and temporal resolution. *Journal of Geophysical Research*, *115*, D15113. <https://doi.org/10.1029/2009JD012257>
- Goldan, P. D., Trainer, M., Kuster, W. C., Parrish, D. D., Carpenter, J., Roberts, J. M., et al. (2012). Measurements of hydrocarbons, oxygenated hydrocarbons, carbon monoxide, and nitrogen oxides in an urban basin in Colorado: Implications for emission inventories. *Journal of Geophysical Research*, *100*, 22,771–22,783. [https://doi.org/10.1029/95JD01369@10.1002/\(ISSN\)2169-8996.PHOTOMS1](https://doi.org/10.1029/95JD01369@10.1002/(ISSN)2169-8996.PHOTOMS1)
- Gourdji, S. M., Mueller, K. L., Yadav, V., Huntzinger, D. N., Andrews, A. E., Trudeau, M., et al. (2012). North American CO<sub>2</sub> exchange: Inter-comparison of modeled estimates with results from a fine-scale atmospheric inversion. *Biogeosciences*, *9*(1), 457–475. <https://doi.org/10.5194/bg-9-457-2012>
- Graven, H. D., Stephens, B. B., Guilderson, T. P., Campos, T. L., Schimel, D. S., Campbell, J. E., & Keeling, R. F. (2009). Vertical profiles of biospheric and fossil fuel-derived CO<sub>2</sub> and fossil fuel CO<sub>2</sub>: CO ratios from airborne measurements of 14c, CO<sub>2</sub> and CO above Colorado, USA. *Tellus B: Chemical and Physical Meteorology*, *61*(3), 536–546. <https://doi.org/10.1111/j.1600-0889.2009.00421.x>
- Guha, A., Gentner, D. R., Weber, R. J., Provencal, R., & Goldstein, A. H. (2015). Source apportionment of methane and nitrous oxide in California's San Joaquin Valley at CalNex 2010 via positive matrix factorization. *Atmospheric Chemistry and Physics*, *15*(20), 12,043–12,063. <https://doi.org/10.5194/acp-15-12043-2015>
- Gurney, K. R., Law, R. M., Denning, A. S., Rayner, P. J., Baker, D., Bousquet, P., et al. (2003). TransCom, 3 CO<sub>2</sub> inversion intercomparison: 1. Annual mean control results and sensitivity to transport and prior flux information. *Tellus B*, *55*(2), 555–579. <https://doi.org/10.1034/j.1600-0889.2003.00049.x>
- Gurney, K. R., Law, R. M., Denning, A. S., Rayner, P. J., Baker, D., Bousquet, P., et al. (2002). Towards robust regional estimates of CO<sub>2</sub> sources and sinks using atmospheric transport models. *Nature*, *415*(6872), 626–630. <https://doi.org/10.1038/415626a>
- Hall, B. D., Dutton, G. S., & Elkins, J. W. (2007). The NOAA nitrous oxide standard scale for atmospheric observations. *Journal of Geophysical Research*, *112*, D09305. <https://doi.org/10.1029/2006JD007954>
- Harley, R. A., Sawyer, R. F., & Milford, J. B. (1997). Updated photochemical modeling for California's South Coast Air Basin: A comparison of chemical mechanisms and motor vehicle emission inventories. *Environmental Science & Technology*, *31*(10), 2829–2839. <https://doi.org/10.1021/es9700562>
- Hayes, D. J., Turner, D. P., Stinson, G., McGuire, A. D., Wei, Y., West, T. O., et al. (2011). Reconciling estimates of the contemporary North American carbon balance among terrestrial biosphere models, atmospheric inversions, and a new approach for estimating net ecosystem exchange from inventory-based data. *Global Change Biology*, *18*(4), 1282–1299. <https://doi.org/10.1111/j.1365-2486.2011.02627.x>
- Hu, L., Montzka, S. A., Miller, J. B., Andrews, A. E., Lehman, S. J., Miller, B. R., et al. (2015). U.S. emissions of HFC-134a derived for 2008–2012 from an extensive flask-air sampling network. *Journal of Geophysical Research: Atmospheres*, *120*, 801–825. <https://doi.org/10.1002/2014JD022617>
- Huntzinger, D., Post, W., Wei, Y., Michalak, A., West, T., Jacobson, A., et al. (2012). North American Carbon Program (NACP) regional interim synthesis: Terrestrial biospheric model intercomparison. *Ecological Modelling*, *232*, 144–157. <https://doi.org/10.1016/j.ecolmodel.2012.02.004>
- Isaac, L. I. D., Lauvaux, T., Davis, K. J., Miles, N. L., Richardson, S. J., Jacobson, A. R., & Andrews, A. E. (2014). Model-data comparison of MCI field campaign atmospheric CO<sub>2</sub> mole fractions. *Journal of Geophysical Research: Atmospheres*, *119*, 10,536–10,551. <https://doi.org/10.1002/2014JD021593>
- Jeong, S., Hsu, Y.-K., Andrews, A. E., Bianco, L., Vaca, P., Wilczak, J. M., & Fischer, M. L. (2013). A multitower measurement network estimate of California's methane emissions. *Journal of Geophysical Research: Atmospheres*, *118*, 11,339–11,35. <https://doi.org/10.1002/jgrd.50854>
- Karion, A., Sweeney, C., Wolter, S., Newberger, T., Chen, H., Andrews, A., et al. (2013). Long-term greenhouse gas measurements from aircraft. *Atmospheric Measurement Techniques*, *6*(3), 511–526. <https://doi.org/10.5194/amt-6-511-2013>
- Kepler, F., Harper, D. B., Röckmann, T., Moore, R. M., & Hamilton, J. T. G. (2005). New insight into the atmospheric chloromethane budget gained using stable carbon isotope ratios. *Atmospheric Chemistry and Physics*, *5*(9), 2403–2411. <https://doi.org/10.5194/acp-5-2403-2005>
- Khalil, M. a. K., Moore, R. M., Harper, D. B., Lobert, J. M., Erickson, D. J., Koropalov, V., et al. (1998). Natural emissions of chlorine-containing gases: Reactive chlorine emissions inventory. *Journal of Geophysical Research*, *104*(D7), 8333–8346. <https://doi.org/10.1029/1998JD100079>
- King, A. W., Andres, R. J., Davis, K. J., Hafer, M., Hayes, D. J., Huntzinger, D. N., et al. (2015). North America's net terrestrial CO<sub>2</sub> exchange with the atmosphere 1990–2009. *Biogeosciences*, *12*(2), 399–414. <https://doi.org/10.5194/bg-12-399-2015>
- King, A. W., Hayes, D. J., Huntzinger, D. N., West, T. O., & Post, W. M. (2012). North American carbon dioxide sources and sinks: Magnitude, attribution, and uncertainty. *Frontiers in Ecology and the Environment*, *10*(10), 512–519. <https://doi.org/10.1890/120066>
- Ko, M. K. W., Sze, N. D., Wang, W.-C., Shia, G., Goldman, A., Murcray, F. J., et al. (1993). Atmospheric sulfur hexafluoride: Sources, sinks and greenhouse warming. *Journal of Geophysical Research*, *98*(D6), 10,499–10,507. <https://doi.org/10.1029/93JD00228>
- Kort, E. A., Eluszkiewicz, J., Stephens, B. B., Miller, J. B., Gerbig, C., Nehrorn, T., et al. (2008). Emissions of CH<sub>4</sub> and N<sub>2</sub>o over the United States and Canada based on a receptor-oriented modeling framework and COBRA-NA atmospheric observations. *Geophysical Research Letters*, *35*, L18808. <https://doi.org/10.1029/2008GL034031>

- LaFranchi, B. W., Pétron, G., Miller, J. B., Lehman, S. J., Andrews, A. E., Dlugokencky, E. J., et al. (2013). Constraints on emissions of carbon monoxide, methane, and a suite of hydrocarbons in the Colorado Front Range using observations of 14 CO<sub>2</sub>. *Atmospheric Chemistry and Physics*, *13*(21), 11,101–11,120. <https://doi.org/10.5194/acp-13-11101-2013>
- Lan, X., Tans, P., Sweeney, C., Andrews, A., Dlugokencky, E., Schwitzke, S., et al. (2019). Long-term measurements show little evidence for large increases in total us methane emissions over the past decade. *Geophysical Research Letters*, *46*, 4991–4999. <https://doi.org/10.1029/2018GL081731>
- Lauvaux, T., & Davis, K. J. (2014). Planetary boundary layer errors in mesoscale inversions of column-integrated CO<sub>2</sub> measurements. *Journal of Geophysical Research: Atmospheres*, *119*, 490–508. <https://doi.org/10.1002/2013JD020175>
- Lauvaux, T., Gioli, B., Sarrat, C., Rayner, P. J., Ciais, P., Chevallier, F., et al. (2009). Bridging the gap between atmospheric concentrations and local ecosystem measurements. *Geophysical Research Letters*, *36*, L19809. <https://doi.org/10.1029/2009GL039574>
- Lauvaux, T., Schuh, A. E., Bocquet, M., Wu, L., Richardson, S., Miles, N., & Davis, K. J. (2012a). Network design for mesoscale inversions of CO<sub>2</sub> sources and sinks. *Tellus B: Chemical and Physical Meteorology*, *64*(1), 17980. <https://doi.org/10.3402/tellusb.v64i0.17980>
- Lauvaux, T., Schuh, A. E., Uliasz, M., Richardson, S., Miles, N., Andrews, A. E., et al. (2012b). Constraining the CO<sub>2</sub> budget of the corn belt: Exploring uncertainties from the assumptions in a mesoscale inverse system. *Atmospheric Chemistry and Physics*, *12*(1), 337–354. <https://doi.org/10.5194/acp-12-337-2012>
- Levin, I., Schuchard, J., Kromer, B., & Münnich, K. O. (1989). The continental European suess effect. *Radiocarbon*, *31*(3), 431–440. <https://doi.org/10.1017/S0033822200012017>
- Levy, H. (1971). Normal atmosphere: Large radical and formaldehyde concentrations predicted. *Science*, *173*(3992), 141–143. <https://doi.org/10.1126/science.173.3992.141>
- Liu, X., Zhang, Y., Huey, L. G., Yokelson, R. J., Wang, Y., Jimenez, J. L., et al. (2016). Agricultural fires in the southeastern U.S. during SEAC4rs: Emissions of trace gases and particles and evolution of ozone, reactive nitrogen, and organic aerosol. *Journal of Geophysical Research: Atmospheres*, *121*, 7383–7414. <https://doi.org/10.1002/2016JD025040>
- Lober, J. M., Keene, W. C., Logan, J. A., & Yevich, R. (1999). Global chlorine emissions from biomass burning: Reactive chlorine emissions inventory. *Journal of Geophysical Research*, *104*, 8373–8389. <https://doi.org/10.1029/1998JD100077>
- Maasakkers, J. D., Jacob, D. J., Sulprizio, M. P., Turner, A. J., Weitz, M., Wirth, T., et al. (2016). Gridded National Inventory of U.S. Methane emissions. *Environmental Science & Technology*, *50*(23), 13,123–13,133. <https://doi.org/10.1021/acs.est.6b02878>
- Masarie, K. A., & Tans, P. P. (1995). Extension and integration of atmospheric carbon dioxide data into a globally consistent measurement record. *Journal of Geophysical Research*, *100*(D6), 11,593–11,610. <https://doi.org/10.1029/95JD00859>
- Miller, J. B., Lehman, S. J., Montzka, S. A., Sweeney, C., Miller, B. R., Karion, A., et al. (2012). Linking emissions of fossil fuel CO<sub>2</sub> and other anthropogenic trace gases using atmospheric 14CO<sub>2</sub>. *Journal of Geophysical Research*, *117*, D08302. <https://doi.org/10.1029/2011JD017048>
- Miller, S. M., Wofsy, S. C., Michalak, A. M., Kort, E. A., Andrews, A. E., Biraud, S. C., et al. (2013). Anthropogenic emissions of methane in the United States. *Proceedings of the National Academy of Sciences of the United States of America*, *110*(50), 20,018–20,022. <https://doi.org/10.1073/pnas.1314392110>
- Montzka, S. A., Calvert, P., Hall, B. D., Elkins, J. W., Conway, T. J., Tans, P. P., & Sweeney, C. (2007). On the global distribution, seasonality, and budget of atmospheric carbonyl sulfide (COS) and some similarities to CO<sub>2</sub>. *Journal of Geophysical Research*, *112*, D09302. <https://doi.org/10.1029/2006JD007665>
- Mosier, A. R. (1998). Closing the global N<sub>2</sub>o budget: Nitrous oxide emissions through the agricultural nitrogen cycle | SpringerLink.
- NASA (2018). Active Fire Data | Earthdata. accessed on 2017-03-10.
- Novelli, P. C., Elkins, J. W., & Steele, L. P. (1991). The development and evaluation of a gravimetric reference scale for measurements of atmospheric carbon monoxide. *Journal of Geophysical Research*, *96*(D7), 13,109–13,121. <https://doi.org/10.1029/91JD01108>
- Novelli, P. C., Lang, P. M., Masarie, K. A., Hurst, D. F., Myers, R., & Elkins, J. W. (1999). Molecular hydrogen in the troposphere: Global distribution and budget. *Journal of Geophysical Research*, *104*(D23), 30,427–30,444. <https://doi.org/10.1029/1999JD900788>
- Olivier, J. G. J., Aardenne, J. A. V., Dentener, F. J., Pagliari, V., Ganzeveld, L. N., & Peters, J. A. H. W. (2005). Recent trends in global greenhouse gas emissions: Regional trends 1970–2000 and spatial distribution of key sources in 2000. *Environmental Sciences*, *2*(2–3), 81–99. <https://doi.org/10.1080/15693430500400345>
- Patra, P. K., Takigawa, M., Dutton, G. S., Uhse, K., Ishijima, K., Lintner, B. R., et al. (2009). Transport mechanisms for synoptic, seasonal and interannual SF<sub>6</sub> variations and “age” of air in troposphere. *Atmospheric Chemistry and Physics*, *9*(4), 1209–1225. <https://doi.org/10.5194/acp-9-1209-2009>
- Peischl, J., Eilerman, S. J., Neuman, J. A., Aikin, K. C., de Gouw, J., Gilman, J. B., et al. (2018). Quantifying methane and ethane emissions to the atmosphere from Central and Western U.S. Oil and natural gas production regions. *Journal of Geophysical Research: Atmospheres*, *123*, 7725–7740. <https://doi.org/10.1029/2018JD028622>
- Peischl, J., Ryerson, T. B., Aikin, K. C., de Gouw, J. A., Gilman, J. B., Holloway, J. S., et al. (2015). Quantifying atmospheric methane emissions from the Haynesville, Fayetteville, and northeastern Marcellus shale gas production regions. *Journal of Geophysical Research: Atmospheres*, *120*, 2119–2139. <https://doi.org/10.1002/2014JD022697>
- Peischl, J., Ryerson, T. B., Brioude, J., Aikin, K. C., Andrews, A. E., Atlas, E., et al. (2013). Quantifying sources of methane using light alkanes in the Los Angeles basin, California. *Journal of Geophysical Research*, *118*, 4974–4990. <https://doi.org/10.1002/jgrd.50413>
- Peters, W., Jacobson, A. R., Sweeney, C., Andrews, A. E., Conway, T. J., Masarie, K., et al. (2007). An atmospheric perspective on north american carbon dioxide exchange: Carbontracker. *Proceedings of the National Academy of Sciences*, *104*(48), 18,925–18,930. <https://doi.org/10.1073/pnas.0708986104>
- Pétron, G., Frost, G., Miller, B. R., Hirsch, A. I., Montzka, S. A., Karion, A., et al. (2012). Hydrocarbon emissions characterization in the Colorado Front Range: A pilot study. *Journal of Geophysical Research*, *117*, D04304. <https://doi.org/10.1029/2011JD016360>
- Peylin, P., Law, R. M., Gurney, K. R., Chevallier, F., Jacobson, A. R., Maki, T., et al. (2013). Global atmospheric carbon budget: Results from an ensemble of atmospheric CO<sub>2</sub> inversions. *Biogeosciences*, *10*, 6699–6720.
- Plant, G., Kort, E. A., Floerchinger, C., Gvakharia, A., Vimont, I., & Sweeney, C. (2019). Large fugitive methane emissions from urban centers along the U.S. East Coast. *Geophysical Research Letters*, *46*, 8500–8507. <https://doi.org/10.1029/2019GL082635>
- Pototsnak, M. J., Wofsy, S. C., Denning, A. S., Conway, T. J., Munger, J. W., & Barnes, D. H. (1999). Influence of biotic exchange and combustion sources on atmospheric CO<sub>2</sub> concentrations in new england from observations at a forest flux tower. *Journal of Geophysical Research*, *104*(D8), 9561–9569. <https://doi.org/10.1029/1999JD900102>
- Rhew, R. C., Miller, B. R., & Weiss, R. F. (2000). Natural methyl bromide and methyl chloride emissions from coastal salt marshes. *Nature*, *403*(6767), 292–295. <https://doi.org/10.1038/35002043>
- Rödenbeck, C., Houweling, S., Gloor, M., & Heimann, M. (2003). CO<sub>2</sub> Flux History 1982–2001 inferred from atmospheric data using a global inversion of atmospheric transport. *Atmospheric Chemistry and Physics*, *3*(6), 1919–1964. <https://doi.org/10.5194/acp-3-1919-2003>

- Schuh, A. E., Denning, A. S., Corbin, K. D., Baker, I. T., Uliasz, M., Parazoo, N., et al. (2010). A regional high-resolution carbon flux inversion of North America for 2004. *Biogeosciences*, 7(5), 1625–1644. <https://doi.org/10.5194/bg-7-1625-2010>
- Schuh, A. E., Jacobson, A. R., Basu, S., Weir, B., Baker, D., Bowman, K., et al. (2019). Quantifying the impact of atmospheric transport uncertainty on CO<sub>2</sub> surface flux estimates. *Global Biogeochemical Cycles*, 33, 484–500. <https://doi.org/10.1029/2018GB006086>
- Schwietzke, S., Griffin, W. M., Matthews, H. S., & Bruhwiler, L. M. P. (2014). Natural gas fugitive emissions rates constrained by global atmospheric methane and ethane. *Environmental Science & Technology*, 48(14), 7714–7722. <https://doi.org/10.1021/es501204c>
- Serça, D., Guenther, A., Klinger, L., Helmig, D., Hereid, D., & Zimmerman, P. (1998). Methyl bromide deposition to soils. *Atmospheric Environment*, 32(9), 1581–1586. [https://doi.org/10.1016/S1352-2310\(97\)00386-5](https://doi.org/10.1016/S1352-2310(97)00386-5)
- Shepherd, M. F., Barzeiti, S., & Hastie, D. R. (1991). The production of atmospheric NO<sub>x</sub> and N<sub>2</sub>O from a fertilized agricultural soil. p. 9.
- Smith, M. L., Gvakharia, A., Kort, E. A., Sweeney, C., Conley, S. A., Faloona, I., et al. (2017). Airborne Quantification of Methane Emissions over the Four Corners region. *Environmental Science and Technology*, 51(10), 5832–5837. <https://doi.org/10.1021/acs.est.6b06107>
- Smith, M. L., Kort, E. A., Karion, A., Sweeney, C., Herndon, S. C., & Yacovitch, T. I. (2015). Airborne ethane observations in the barnett shale: Quantification of ethane flux and attribution of methane emissions. *Environmental Science & Technology*, 49(13), 8158–8166. <https://doi.org/10.1021/acs.est.5b00219>
- Stephens, B. B., Gurney, K. R., Tans, P. P., Sweeney, C., Peters, W., Bruhwiler, L., et al. (2007). Weak northern and strong tropical land carbon uptake from vertical profiles of atmospheric CO<sub>2</sub>. *Science*, 316(5832), 1732–1735. <https://doi.org/10.1126/science.1137004>
- Swarthout, R. F., Russo, R. S., Zhou, Y., Hart, A. H., & Sive, B. C. (2013). Volatile organic compound distributions during the NACHTT campaign at the Boulder Atmospheric Observatory: Influence of urban and natural gas sources. *Journal of Geophysical Research: Atmospheres*, 118, 10,614–10,637. <https://doi.org/10.1002/jgrd.50722>
- Sweeney, C., Karion, A., Wolter, S., Newberger, T., Guenther, D., Higgs, J. A., et al. (2015). Seasonal climatology of CO<sub>2</sub> across North America from aircraft measurements in the NOAA/ESRL Global Greenhouse Gas Reference Network. *Journal of Geophysical Research: Atmospheres*, 120, 5155–5190. <https://doi.org/10.1002/2014JD022591>
- Tans, P. P., Fung, I. Y., & Takahashi, T. (1990). Observational constraints on the global atmospheric CO<sub>2</sub> budget. *Science*, 247(4949), 1431–1438. <https://doi.org/10.1126/science.247.4949.1431>
- Thompson, C. R., Hueber, J., & Helmig, D. (2014). Influence of oil and gas emissions on ambient atmospheric non-methane hydrocarbons in residential areas of Northeastern Colorado. *Elementa: Science of the Anthropocene*, 3, 000035. <https://doi.org/10.12952/journal.elementa.000035>
- Thoning, K. W., Tans, P. P., & Komhyr, W. D. (1989). Atmospheric carbon dioxide at Mauna Loa Observatory: 2. Analysis of the NOAA GMCC data, 1974–1985. *Journal of Geophysical Research*, 94(D6), 8549–8565. <https://doi.org/10.1029/JD094iD06p08549>
- Tian, D., Hu, Y., Wang, Y., Boylan, J. W., Zheng, M., & Russell, A. G. (2009). Assessment of biomass burning emissions and their impacts on urban and regional PM<sub>2.5</sub>: A Georgia case study. *Environmental Science & Technology*, 43(2), 299–305. <https://doi.org/10.1021/es801827s>
- Turnbull, J. C., Karion, A., Davis, K. J., Lauvaux, T., Miles, N. L., Richardson, S. J., et al. (2019). Synthesis of urban CO<sub>2</sub> emission estimates from multiple methods from the Indianapolis flux project (influx). *Environmental Science & Technology*, 53(1), 287–295. <https://doi.org/10.1021/acs.est.8b05552>
- Turnbull, J. C., Karion, A., Fischer, M. L., Faloona, I., Guilderson, T., Lehman, S. J., et al. (2011). Assessment of fossil fuel carbon dioxide and other anthropogenic trace gas emissions from airborne measurements over Sacramento, California in spring 2009. *Atmospheric Chemistry and Physics*, 11(2), 705–721. <https://doi.org/10.5194/acp-11-705-2011>
- Turnbull, J. C., Miller, J. B., Lehman, S. J., Tans, P. P., Sparks, R. J., & Southon, J. (2006). Comparison of <sup>14</sup>CO<sub>2</sub>, CO, and SF<sub>6</sub> as tracers for recently added fossil fuel CO<sub>2</sub> in the atmosphere and implications for biological CO<sub>2</sub> exchange. *Geophysical Research Letters*, 33, L01817. <https://doi.org/10.1029/2005GL024213>
- Turnbull, J. C., Sweeney, C., Karion, A., Newberger, T., Lehman, S. J., Tans, P. P., et al. (2014). Toward quantification and source sector identification of fossil fuel CO<sub>2</sub> emissions from an urban area: Results from the INFLUX experiment. *Journal of Geophysical Research: Atmospheres*, 120, 292–312. <https://doi.org/10.1002/2014JD022551>
- US EPA (2016). Gridded 2012 Methane Emissions. <https://www.epa.gov/ghgemissions/gridded-2012-methane-emissions>
- USGS (2019). Eastern U.S. Remote Sensing Phenology Data. <https://doi.org/10.5066/F7PC30G1>, Date accessed: 1-21-2019.
- United Nations Environment Programme (2019). The Montreal protocol on substances that deplete the ozone layer | ozone secretariat.
- Varner, R. K. (1999). Wetlands: A potentially significant source of atmospheric methyl bromide and methyl chloride - Varner - 1999 - Geophysical Research Letters - Wiley Online Library.
- WMO (2013). [gaw\\_213\\_en.pdf](https://www.wmo.int/pages/prog/arep/ghg/ghg_gaw_213_en.pdf), GAW Report 213.
- Warneke, C., McKeen, S. A., de Gouw, J. A., Goldan, P. D., Kuster, W. C., Holloway, J. S., et al. (2007). Determination of urban volatile organic compound emission ratios and comparison with an emissions database. *Journal of Geophysical Research*, 112, D10S47. <https://doi.org/10.1029/2006JD007930>
- Zhang, X., Hecobian, A., Zheng, M., Frank, N. H., & Weber, R. J. (2010). Biomass burning impact on PM<sub>2.5</sub> over the southeastern US during 2007: Integrating chemically speciated FRM filter measurements, MODIS, fire counts and PMF analysis. *Atmospheric Chemistry and Physics*, 10(14), 6839–6853. <https://doi.org/10.5194/acp-10-6839-2010>
- Zhao, C., Andrews, A. E., Bianco, L., Eluszkiewicz, J., Hirsch, A., MacDonald, C., et al. (2009). Atmospheric inverse estimates of methane emissions from Central California. *Journal of Geophysical Research*, 114, D16302. <https://doi.org/10.1029/2008JD011671>
- Zhao, C. L., & Tans, P. P. (2006). Estimating uncertainty of the WMO mole fraction scale for carbon dioxide in air. *Journal of Geophysical Research*, 111, D08S09. <https://doi.org/10.1029/2005JD006003>